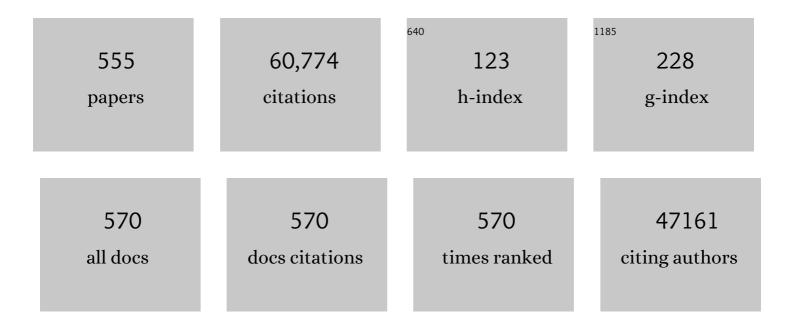
## Michael F Toney

List of Publications by Year in descending order

Source: https://exaly.com/author-pdf/5990650/publications.pdf Version: 2024-02-01



#	Article	IF	CITATIONS
1	Lattice-strain control of the activity in dealloyed core–shell fuel cell catalysts. Nature Chemistry, 2010, 2, 454-460.	6.6	2,489
2	Pathways for practical high-energy long-cycling lithium metal batteries. Nature Energy, 2019, 4, 180-186.	19.8	2,101
3	Liquid-crystalline semiconducting polymers with high charge-carrier mobility. Nature Materials, 2006, 5, 328-333.	13.3	2,001
4	A general relationship between disorder, aggregation and charge transport in conjugated polymers. Nature Materials, 2013, 12, 1038-1044.	13.3	1,742
5	Ultra-high mobility transparent organic thin film transistors grown by an off-centre spin-coating method. Nature Communications, 2014, 5, 3005.	5.8	1,155
6	Quantitative Determination of Organic Semiconductor Microstructure from the Molecular to Device Scale. Chemical Reviews, 2012, 112, 5488-5519.	23.0	1,133
7	Dependence of Regioregular Poly(3-hexylthiophene) Film Morphology and Field-Effect Mobility on Molecular Weight. Macromolecules, 2005, 38, 3312-3319.	2.2	1,003
8	Metal Oxide Surfaces and Their Interactions with Aqueous Solutions and Microbial Organisms. Chemical Reviews, 1999, 99, 77-174.	23.0	981
9	Tuning charge transport in solution-sheared organic semiconductors using lattice strain. Nature, 2011, 480, 504-508.	13.7	981
10	A highly stretchable, transparent, and conductive polymer. Science Advances, 2017, 3, e1602076.	4.7	962
11	Highly oriented crystals at the buried interface in polythiophene thin-film transistors. Nature Materials, 2006, 5, 222-228.	13.3	737
12	Siloxane-Terminated Solubilizing Side Chains: Bringing Conjugated Polymer Backbones Closer and Boosting Hole Mobilities in Thin-Film Transistors. Journal of the American Chemical Society, 2011, 133, 20130-20133.	6.6	628
13	High-Capacity Micrometer-Sized Li <sub>2</sub> S Particles as Cathode Materials for Advanced Rechargeable Lithium-Ion Batteries. Journal of the American Chemical Society, 2012, 134, 15387-15394.	6.6	624
14	Interdiffusion of PCBM and P3HT Reveals Miscibility in a Photovoltaically Active Blend. Advanced Energy Materials, 2011, 1, 82-89.	10.2	572
15	Band Gap Tuning via Lattice Contraction and Octahedral Tilting in Perovskite Materials for Photovoltaics. Journal of the American Chemical Society, 2017, 139, 11117-11124.	6.6	570
16	Voltage-dependent ordering of water molecules at an electrode–electrolyte interface. Nature, 1994, 368, 444-446.	13.7	566
17	Crystalline Ultrasmooth Self-Assembled Monolayers of Alkylsilanes for Organic Field-Effect Transistors. Journal of the American Chemical Society, 2009, 131, 9396-9404.	6.6	562
18	Effects of Thermal Annealing Upon the Morphology of Polymer–Fullerene Blends. Advanced Functional Materials. 2010. 20. 3519-3529.	7.8	539

#	Article	IF	CITATIONS
19	In Operando X-ray Diffraction and Transmission X-ray Microscopy of Lithium Sulfur Batteries. Journal of the American Chemical Society, 2012, 134, 6337-6343.	6.6	475
20	Coupling between oxygen redox and cation migration explains unusual electrochemistry in lithium-rich layered oxides. Nature Communications, 2017, 8, 2091.	5.8	469
21	Side-Chain Tunability of Furan-Containing Low-Band-Gap Polymers Provides Control of Structural Order in Efficient Solar Cells. Journal of the American Chemical Society, 2012, 134, 2180-2185.	6.6	458
22	Direct observation of the alignment of ferromagnetic spins by antiferromagnetic spins. Nature, 2000, 405, 767-769.	13.7	441
23	Full open-framework batteries for stationary energy storage. Nature Communications, 2014, 5, 3007.	5.8	440
24	Large modulation of carrier transport by grain-boundary molecular packing and microstructure in organic thin films. Nature Materials, 2009, 8, 952-958.	13.3	416
25	Structural Characterization of a Pentacene Monolayer on an Amorphous SiO2Substrate with Grazing Incidence X-ray Diffraction. Journal of the American Chemical Society, 2004, 126, 4084-4085.	6.6	412
26	The Importance of Fullerene Percolation in the Mixed Regions of Polymer–Fullerene Bulk Heterojunction Solar Cells. Advanced Energy Materials, 2013, 3, 364-374.	10.2	412
27	Dynamics of pore formation during laser powder bed fusion additive manufacturing. Nature Communications, 2019, 10, 1987.	5.8	408
28	The Influence of Poly(3-hexylthiophene) Regioregularity on Fullerene-Composite Solar Cell Performance. Journal of the American Chemical Society, 2008, 130, 16324-16329.	6.6	394
29	Bimolecular Crystals of Fullerenes in Conjugated Polymers and the Implications of Molecular Mixing for Solar Cells. Advanced Functional Materials, 2009, 19, 1173-1179.	7.8	392
30	Molecular Packing of High-Mobility Diketo Pyrrolo-Pyrrole Polymer Semiconductors with Branched Alkyl Side Chains. Journal of the American Chemical Society, 2011, 133, 15073-15084.	6.6	381
31	Near-surface alignment of polymers in rubbed films. Nature, 1995, 374, 709-711.	13.7	373
32	Hybrid Organic–Inorganic Perovskites (HOIPs): Opportunities and Challenges. Advanced Materials, 2015, 27, 5102-5112.	11.1	372
33	High-performance sodium–organic battery by realizing four-sodium storage in disodium rhodizonate. Nature Energy, 2017, 2, 861-868.	19.8	372
34	Direct Observation of Structural Evolution of Metal Chalcogenide in Electrocatalytic Water Oxidation. ACS Nano, 2018, 12, 12369-12379.	7.3	366
35	X-ray Scattering Study of Thin Films of Poly(2,5-bis(3-alkylthiophen-2-yl)thieno[3,2-b]thiophene). Journal of the American Chemical Society, 2007, 129, 3226-3237.	6.6	351
36	Mechanism of Tin Oxidation and Stabilization by Lead Substitution in Tin Halide Perovskites. ACS Energy Letters, 2017, 2, 2159-2165.	8.8	351

#	Article	IF	CITATIONS
37	Compositional and orientational control in metal halide perovskites of reduced dimensionality. Nature Materials, 2018, 17, 900-907.	13.3	351
38	Solvent Additives: Key Morphologyâ€Directing Agents for Solutionâ€Processed Organic Solar Cells. Advanced Materials, 2018, 30, e1707114.	11.1	346
39	Unconventional Faceâ€On Texture and Exceptional Inâ€Plane Order of a High Mobility nâ€Type Polymer. Advanced Materials, 2010, 22, 4359-4363.	11.1	344
40	The meniscus-guided deposition of semiconducting polymers. Nature Communications, 2018, 9, 534.	5.8	324
41	Critical Role of Side-Chain Attachment Density on the Order and Device Performance of Polythiophenes. Macromolecules, 2007, 40, 7960-7965.	2.2	321
42	Quantification of Thin Film Crystallographic Orientation Using X-ray Diffraction with an Area Detector. Langmuir, 2010, 26, 9146-9151.	1.6	315
43	Chargeâ€Transport Anisotropy Due to Grain Boundaries in Directionally Crystallized Thin Films of Regioregular Poly(3â€hexylthiophene). Advanced Materials, 2009, 21, 1568-1572.	11.1	305
44	Anisotropic Structure and Charge Transport in Highly Strainâ€Aligned Regioregular Poly(3â€hexylthiophene). Advanced Functional Materials, 2011, 21, 3697-3705.	7.8	288
45	Defect-Induced Band-Edge Reconstruction of a Bismuth-Halide Double Perovskite for Visible-Light Absorption. Journal of the American Chemical Society, 2017, 139, 5015-5018.	6.6	288
46	Metal–oxygen decoordination stabilizes anion redox in Li-rich oxides. Nature Materials, 2019, 18, 256-265.	13.3	280
47	Drastic Control of Texture in a High Performance n-Type Polymeric Semiconductor and Implications for Charge Transport. Macromolecules, 2011, 44, 5246-5255.	2.2	278
48	Perpendicular magnetic anisotropy and magnetic domain structure in sputtered epitaxial FePt (001) L10 films. Journal of Applied Physics, 1998, 84, 5686-5692.	1.1	275
49	A map of the inorganic ternary metal nitrides. Nature Materials, 2019, 18, 732-739.	13.3	274
50	Control of the axis of chemical ordering and magnetic anisotropy in epitaxial FePt films. Journal of Applied Physics, 1996, 79, 5967.	1.1	272
51	Engineering Stress in Perovskite Solar Cells to Improve Stability. Advanced Energy Materials, 2018, 8, 1802139.	10.2	271
52	Quantitative analysis of lattice disorder and crystallite size in organic semiconductor thin films. Physical Review B, 2011, 84, .	1.1	262
53	Molecular Order in High-Efficiency Polymer/Fullerene Bulk Heterojunction Solar Cells. ACS Nano, 2011, 5, 8248-8257.	7.3	260
54	The chemical and structural origin of efficient p-type doping in P3HT. Organic Electronics, 2013, 14, 1330-1336.	1.4	256

#	Article	IF	CITATIONS
55	Chloride in Lead Chloride-Derived Organo-Metal Halides for Perovskite-Absorber Solar Cells. Chemistry of Materials, 2014, 26, 7158-7165.	3.2	256
56	Temperature dependent magnetic properties of highly chemically ordered Fe[sub 55â^'x]Ni[sub x]Pt[sub 45]L1[sub 0] films. Journal of Applied Physics, 2002, 91, 6595.	1.1	253
57	Structural Order in Bulk Heterojunction Films Prepared with Solvent Additives. Advanced Materials, 2011, 23, 2284-2288.	11.1	248
58	Ultrahigh electrical conductivity in solution-sheared polymeric transparent films. Proceedings of the United States of America, 2015, 112, 14138-14143.	3.3	248
59	Tuning the Properties of Polymer Bulk Heterojunction Solar Cells by Adjusting Fullerene Size to Control Intercalation. Nano Letters, 2009, 9, 4153-4157.	4.5	243
60	Device-Scale Perpendicular Alignment of Colloidal Nanorods. Nano Letters, 2010, 10, 195-201.	4.5	241
61	The Structure of the Passive Film That Forms on Iron in Aqueous Environments. Journal of the Electrochemical Society, 2000, 147, 2162.	1.3	232
62	The Role of OTS Density on Pentacene and C <sub>60</sub> Nucleation, Thin Film Growth, and Transistor Performance. Advanced Functional Materials, 2009, 19, 1962-1970.	7.8	227
63	Surface regulation enables high stability of single-crystal lithium-ion cathodes at high voltage. Nature Communications, 2020, 11, 3050.	5.8	225
64	Flow-enhanced solution printing of all-polymer solar cells. Nature Communications, 2015, 6, 7955.	5.8	221
65	Relationships between Lead Halide Perovskite Thin-Film Fabrication, Morphology, and Performance in Solar Cells. Journal of the American Chemical Society, 2016, 138, 463-470.	6.6	221
66	Observation of Transient Structural-Transformation Dynamics in a Cu <sub>2</sub> S Nanorod. Science, 2011, 333, 206-209.	6.0	220
67	Molecular Characterization of Organic Electronic Films. Advanced Materials, 2011, 23, 319-337.	11.1	215
68	Low-Dielectric, Nanoporous Organosilicate Films Prepared via Inorganic/Organic Polymer Hybrid Templates. Chemistry of Materials, 1999, 11, 3080-3085.	3.2	214
69	Rollâ€ŧoâ€Roll Printed Largeâ€Area Allâ€Polymer Solar Cells with 5% Efficiency Based on a Low Crystallinity Conjugated Polymer Blend. Advanced Energy Materials, 2017, 7, 1602742.	10.2	214
70	Electrochemical Deposition of Copper on a Gold Electrode in Sulfuric Acid: Resolution of the Interfacial Structure. Physical Review Letters, 1995, 75, 4472-4475.	2.9	213
71	p-Channel Organic Semiconductors Based on Hybrid Aceneâ^'Thiophene Molecules for Thin-Film Transistor Applications. Journal of the American Chemical Society, 2005, 127, 3997-4009.	6.6	204
72	Size-Dependent Lattice Structure and Confinement Properties in CsPbl <sub>3</sub> Perovskite Nanocrystals: Negative Surface Energy for Stabilization. ACS Energy Letters, 2020, 5, 238-247.	8.8	201

#	Article	IF	CITATIONS
73	Impact of interfacial molecular orientation on radiative recombination and charge generation efficiency. Nature Communications, 2017, 8, 79.	5.8	198
74	Ultrafast Growth of Highly Branched Palladium Nanostructures for Catalysis. ACS Nano, 2010, 4, 396-402.	7.3	194
75	Enhanced Solid-State Order and Field-Effect Hole Mobility through Control of Nanoscale Polymer Aggregation. Journal of the American Chemical Society, 2013, 135, 19229-19236.	6.6	194
76	Controlling Solutionâ€Phase Polymer Aggregation with Molecular Weight and Solvent Additives to Optimize Polymerâ€Fullerene Bulk Heterojunction Solar Cells. Advanced Energy Materials, 2014, 4, 1301733.	10.2	194
77	Magneto-optical Kerr spectroscopy of a new chemically ordered alloy:Co3Pt. Physical Review Letters, 1993, 71, 2493-2496.	2.9	193
78	On the relationship of magnetocrystalline anisotropy and stoichiometry in epitaxial L10 CoPt (001) and FePt (001) thin films. Journal of Applied Physics, 2005, 98, 033904.	1.1	190
79	Atomic Structure of the Passive Oxide Film Formed on Iron. Physical Review Letters, 1997, 79, 4282-4285.	2.9	189
80	Structure-Activity-Stability Relationships of Ptâ^'Co Alloy Electrocatalysts in Gas-Diffusion Electrode Layers. Journal of Physical Chemistry C, 2007, 111, 3744-3752.	1.5	188
81	Designing a Quinone-Based Redox Mediator to Facilitate Li2S Oxidation in Li-S Batteries. Joule, 2019, 3, 872-884.	11.7	188
82	Reversible Multivalent (Monovalent, Divalent, Trivalent) Ion Insertion in Open Framework Materials. Advanced Energy Materials, 2015, 5, 1401869.	10.2	185
83	Effect of Al <sub>2</sub> O <sub>3</sub> Coating on Stabilizing LiNi <sub>0.4</sub> Mn <sub>0.4</sub> Co <sub>0.2</sub> O <sub>2</sub> Cathodes. Chemistry of Materials, 2015, 27, 6146-6154.	3.2	185
84	Solid Electrolyte Interphase on Native Oxide-Terminated Silicon Anodes for Li-Ion Batteries. Joule, 2019, 3, 762-781.	11.7	185
85	Impact of Surfaces on Photoinduced Halide Segregation in Mixed-Halide Perovskites. ACS Energy Letters, 2018, 3, 2694-2700.	8.8	184
86	Precise Structure of Pentacene Monolayers on Amorphous Silicon Oxide and Relation to Charge Transport. Advanced Materials, 2009, 21, 2294-2298.	11.1	183
87	Morphologyâ€Dependent Trap Formation in High Performance Polymer Bulk Heterojunction Solar Cells. Advanced Energy Materials, 2011, 1, 954-962.	10.2	183
88	Interfacial Segregation in Polymer/Fullerene Blend Films for Photovoltaic Devices. Macromolecules, 2010, 43, 3828-3836.	2.2	182
89	Structural origin of gap states in semicrystalline polymers and the implications for charge transport. Physical Review B, 2011, 83, .	1.1	180
90	Manganese–cobalt hexacyanoferrate cathodes for sodium-ion batteries. Journal of Materials Chemistry A, 2016, 4, 4211-4223.	5.2	180

#	Article	IF	CITATIONS
91	A modular molecular framework for utility in small-molecule solution-processed organic photovoltaic devices. Journal of Materials Chemistry, 2011, 21, 12700.	6.7	175
92	How Nanoparticles Coalesce: An in Situ Study of Au Nanoparticle Aggregation and Grain Growth. Chemistry of Materials, 2011, 23, 3312-3317.	3.2	174
93	Structure of Dealloyed PtCu3Thin Films and Catalytic Activity for Oxygen Reduction. Chemistry of Materials, 2010, 22, 4712-4720.	3.2	173
94	Electrochemical trapping of metastable Mn <sup>3+</sup> ions for activation of MnO <sub>2</sub> oxygen evolution catalysts. Proceedings of the National Academy of Sciences of the United States of America, 2018, 115, E5261-E5268.	3.3	173
95	Surface and grain-boundary scattering in nanometric Cu films. Physical Review B, 2010, 81, .	1.1	172
96	Manipulating the Morphology of P3HT–PCBM Bulk Heterojunction Blends with Solvent Vapor Annealing. Chemistry of Materials, 2012, 24, 3923-3931.	3.2	171
97	Distribution of water molecules at Ag(111)/electrolyte interface as studied with surface X-ray scattering. Surface Science, 1995, 335, 326-332.	0.8	167
98	Tin–lead halide perovskites with improved thermal and air stability for efficient all-perovskite tandem solar cells. Sustainable Energy and Fuels, 2018, 2, 2450-2459.	2.5	167
99	Crystallization in one-step solution deposition of perovskite films: Upward or downward?. Science Advances, 2021, 7, .	4.7	165
100	Molecular Interactions and Ordering in Electrically Doped Polymers: Blends of PBTTT and F <sub>4</sub> TCNQ. Macromolecules, 2014, 47, 6836-6846.	2.2	164
101	Effect of chemical pressure on the charge density wave transition in rare-earth tritellurides <mml:math <br="" xmlns:mml="http://www.w3.org/1998/Math/MathML">display="inline"&gt;<mml:mrow><mml:mi>R</mml:mi><mml:msub><mml:mi mathvariant="normal"&gt;Te<mml:mn>3</mml:mn></mml:mi </mml:msub></mml:mrow></mml:math> .	1.1	163
102	Physical Review B, 2008, 77, . Controlling the Orientation of Terraced Nanoscale "Ribbons―of a Poly(thiophene) Semiconductor. ACS Nano, 2009, 3, 780-787.	7.3	160
103	Activity–stability relationships of ordered and disordered alloy phases of Pt3Co electrocatalysts for the oxygen reduction reaction (ORR). Electrochimica Acta, 2007, 52, 2765-2774.	2.6	159
104	Grazing incidence x-ray diffraction of lead monolayers at a silver (111) and gold (111) electrode/electrolyte interface. The Journal of Physical Chemistry, 1988, 92, 220-225.	2.9	158
105	In Situ and Ex Situ Studies of Platinum Nanocrystals: Growth and Evolution in Solution. Journal of the American Chemical Society, 2009, 131, 14590-14595.	6.6	157
106	<i>In Situ</i> X-ray Diffraction Studies of (De)lithiation Mechanism in Silicon Nanowire Anodes. ACS Nano, 2012, 6, 5465-5473.	7.3	156
107	P2–Na <sub><i>x</i></sub> Co <sub><i>y</i></sub> Mn <sub>1–<i>y</i></sub> O <sub>2</sub> ( <i>y</i> = Cycling Stability. Chemistry of Materials, 2016, 28, 2041-2051.	0,) Tj ETQq 3.2	1 1 0.78431 154
108	Thermal engineering of FAPbI3 perovskite material via radiative thermal annealing and in situ XRD. Nature Communications, 2017, 8, 14075.	5.8	149

#	Article	IF	CITATIONS
109	Simple Synthesis and Functionalization of Iron Nanoparticles for Magnetic Resonance Imaging. Angewandte Chemie - International Edition, 2011, 50, 4206-4209.	7.2	148
110	Controlling Thin-Film Stress and Wrinkling during Perovskite Film Formation. ACS Energy Letters, 2018, 3, 1225-1232.	8.8	148
111	A Mechanistic Understanding of Processing Additiveâ€Induced Efficiency Enhancement in Bulk Heterojunction Organic Solar Cells. Advanced Materials, 2014, 26, 300-305.	11.1	145
112	Growth temperature dependence of longâ€range alloy order and magnetic properties of epitaxial FexPt1â^'x (xâ‰,0.5) films. Applied Physics Letters, 1996, 69, 1166-1168.	1.5	143
113	Fine-Tuning Semiconducting Polymer Self-Aggregation and Crystallinity Enables Optimal Morphology and High-Performance Printed All-Polymer Solar Cells. Journal of the American Chemical Society, 2020, 142, 392-406.	6.6	143
114	Controlling Nucleation and Crystallization in Solutionâ€Processed Organic Semiconductors for Thinâ€Film Transistors. Advanced Materials, 2009, 21, 3605-3609.	11.1	141
115	Synthesis, Alignment, and Magnetic Properties of Monodisperse Nickel Nanocubes. Journal of the American Chemical Society, 2012, 134, 855-858.	6.6	141
116	Molecular Packing and Solar Cell Performance in Blends of Polymers with a Bisadduct Fullerene. Nano Letters, 2012, 12, 1566-1570.	4.5	140
117	Enhanced Vertical Charge Transport in a Semiconducting P3HT Thin Film on Single Layer Graphene. Advanced Functional Materials, 2015, 25, 664-670.	7.8	138
118	Significant dependence of morphology and charge carrier mobility on substrate surface chemistry in high performance polythiophene semiconductor films. Applied Physics Letters, 2007, 90, 062117.	1.5	136
119	Grazing incidence x-ray scattering studies of thin films of an aromatic polyimide. Macromolecules, 1993, 26, 2847-2859.	2.2	131
120	Orientational Ordering of Nitrogen Molecular Axes for a Commensurate Monolayer Physisorbed on Graphite. Physical Review Letters, 1982, 48, 177-180.	2.9	130
121	Narrow-Band-Gap Conjugated Chromophores with Extended Molecular Lengths. Journal of the American Chemical Society, 2012, 134, 20609-20612.	6.6	128
122	Structural Origins of Light-Induced Phase Segregation in Organic-Inorganic Halide Perovskite Photovoltaic Materials. Matter, 2020, 2, 207-219.	5.0	128
123	Use of Xâ€Ray Diffraction, Molecular Simulations, and Spectroscopy to Determine the Molecular Packing in a Polymerâ€Fullerene Bimolecular Crystal. Advanced Materials, 2012, 24, 6071-6079.	11.1	126
124	Time-Resolved Structural Evolution of Additive-Processed Bulk Heterojunction Solar Cells. Journal of the American Chemical Society, 2012, 134, 2884-2887.	6.6	125
125	An instrument for <i>in situ</i> time-resolved X-ray imaging and diffraction of laser powder bed fusion additive manufacturing processes. Review of Scientific Instruments, 2018, 89, 055101.	0.6	123
126	Insitu nanotomography and operando transmission X-ray microscopy of micron-sized Ge particles. Energy and Environmental Science, 2014, 7, 2771-2777.	15.6	117

#	Article	IF	CITATIONS
127	Perovskite-Inspired Photovoltaic Materials: Toward Best Practices in Materials Characterization and Calculations. Chemistry of Materials, 2017, 29, 1964-1988.	3.2	116
128	Molecular Basis of Mesophase Ordering in a Thiophene-Based Copolymer. Macromolecules, 2008, 41, 5709-5715.	2.2	114
129	A Review of Existing and Emerging Methods for Lithium Detection and Characterization in Liâ€lon and Liâ€Metal Batteries. Advanced Energy Materials, 2021, 11, 2100372.	10.2	114
130	Surface-induced ordering of an aromatic polyimide. Physical Review Letters, 1991, 66, 1181-1184.	2.9	112
131	Understanding Phase Transformation in Crystalline Ge Anodes for Li-Ion Batteries. Chemistry of Materials, 2014, 26, 3739-3746.	3.2	112
132	Size Dependence of a Temperature-Induced Solid–Solid Phase Transition in Copper(I) Sulfide. Journal of Physical Chemistry Letters, 2011, 2, 2402-2406.	2.1	111
133	Control of the Electrical Properties in Spinel Oxides by Manipulating the Cation Disorder. Advanced Functional Materials, 2014, 24, 610-618.	7.8	109
134	Three-Dimensional Packing Structure and Electronic Properties of Biaxially Oriented Poly(2,5-bis(3-alkylthiophene-2-yl)thieno[3,2- <i>b</i> ]thiophene) Films. Journal of the American Chemical Society, 2012, 134, 6177-6190.	6.6	108
135	Vertically Segregated Structure and Properties of Small Molecule–Polymer Blend Semiconductors for Organic Thinâ€Film Transistors. Advanced Functional Materials, 2013, 23, 366-376.	7.8	106
136	The formation mechanism for printed silver-contacts for silicon solar cells. Nature Communications, 2016, 7, 11143.	5.8	106
137	Persistent and partially mobile oxygen vacancies in Li-rich layered oxides. Nature Energy, 2021, 6, 642-652.	19.8	106
138	The use of poly-cation oxides to lower the temperature of two-step thermochemical water splitting. Energy and Environmental Science, 2018, 11, 2172-2178.	15.6	105
139	Correlating the scattered intensities of P3HT and PCBM to the current densities of polymer solar cells. Chemical Communications, 2011, 47, 436-438.	2.2	103
140	Poly(3-hexylthiophene) and [6,6]-Phenyl-C <sub>61</sub> -butyric Acid Methyl Ester Mixing in Organic Solar Cells. Macromolecules, 2012, 45, 6587-6599.	2.2	103
141	In-situ grazing incidence X-ray diffraction study of electrochemically deposited Pb monolayers on Ag(111). Surface Science, 1988, 193, L29-L36.	0.8	102
142	Versatile Interpenetrating Polymer Network Approach to Robust Stretchable Electronic Devices. Chemistry of Materials, 2017, 29, 7645-7652.	3.2	101
143	Fictitious phase separation in Li layered oxides driven by electro-autocatalysis. Nature Materials, 2021, 20, 991-999.	13.3	101
144	Thickness and growth temperature dependence of structure and magnetism in FePt thin films. Journal of Applied Physics, 2003, 93, 9902-9907.	1.1	100

#	Article	IF	CITATIONS
145	Structure and Mechanism of Strength Enhancement in Interpenetrating Polymer Network Hydrogels. Macromolecules, 2011, 44, 5776-5787.	2.2	100
146	Role of confinement and aggregation in charge transport in semicrystalline polythiophene thin films. Physical Review B, 2012, 86, .	1.1	100
147	Real-Time Observation of Poly(3-alkylthiophene) Crystallization and Correlation with Transient Optoelectronic Properties. Macromolecules, 2011, 44, 6653-6658.	2.2	99
148	Novel ALD Chemistry Enabled Low-Temperature Synthesis of Lithium Fluoride Coatings for Durable Lithium Anodes. ACS Applied Materials & Interfaces, 2018, 10, 26972-26981.	4.0	99
149	Dominant role of grain boundary scattering in the resistivity of nanometric Cu films. Physical Review B, 2009, 79, .	1.1	98
150	Understanding crystallization pathways leading to manganese oxide polymorph formation. Nature Communications, 2018, 9, 2553.	5.8	98
151	Factors Governing Intercalation of Fullerenes and Other Small Molecules Between the Side Chains of Semiconducting Polymers Used in Solar Cells. Advanced Energy Materials, 2012, 2, 1208-1217.	10.2	97
152	Synthesis, Properties, and Electronic Applications of Size-Controlled Poly(3-hexylthiophene) Nanoparticles. Langmuir, 2010, 26, 13056-13061.	1.6	95
153	Charge Transport in Highly Face-On Poly(3-hexylthiophene) Films. Journal of Physical Chemistry C, 2013, 117, 17421-17428.	1.5	95
154	Emerging In Situ and Operando Nanoscale Xâ€Ray Imaging Techniques for Energy Storage Materials. Advanced Functional Materials, 2015, 25, 1622-1637.	7.8	95
155	Mixing Behavior in Small Molecule:Fullerene Organic Photovoltaics. Chemistry of Materials, 2017, 29, 3062-3069.	3.2	94
156	X-ray depth profiling of iron oxide thin films. Journal of Materials Research, 1988, 3, 351-356.	1.2	93
157	Phase, grain structure, stress, and resistivity of sputter-deposited tungsten films. Journal of Vacuum Science and Technology A: Vacuum, Surfaces and Films, 2011, 29, .	0.9	93
158	Effect of Solution Shearing Method on Packing and Disorder of Organic Semiconductor Polymers. Chemistry of Materials, 2015, 27, 2350-2359.	3.2	92
159	Chlorine in PbCl <sub>2</sub> -Derived Hybrid-Perovskite Solar Absorbers. Chemistry of Materials, 2015, 27, 7240-7243.	3.2	91
160	Effect of Nonâ€Chlorinated Mixed Solvents on Charge Transport and Morphology of Solutionâ€Processed Polymer Fieldâ€Effect Transistors. Advanced Functional Materials, 2014, 24, 3524-3534.	7.8	89
161	Effects of Molecular Structure and Packing Order on the Stretchability of Semicrystalline Conjugated Poly(Tetrathienoaceneâ€diketopyrrolopyrrole) Polymers. Advanced Electronic Materials, 2017, 3, 1600311.	2.6	89
162	Scalable and Selective Dispersion of Semiconducting Arc-Discharged Carbon Nanotubes by Dithiafulvalene/Thiophene Copolymers for Thin Film Transistors. ACS Nano, 2013, 7, 2659-2668.	7.3	88

#	Article	IF	CITATIONS
163	Evolution of Iodoplumbate Complexes in Methylammonium Lead Iodide Perovskite Precursor Solutions. Chemistry of Materials, 2017, 29, 1315-1320.	3.2	88
164	Confined Interlayer Water Promotes Structural Stability for High-Rate Electrochemical Proton Intercalation in Tungsten Oxide Hydrates. ACS Energy Letters, 2019, 4, 2805-2812.	8.8	88
165	Structural and spectral dynamics of single-crystalline Ruddlesden-Popper phase halide perovskite blue light-emitting diodes. Science Advances, 2020, 6, eaay4045.	4.7	88
166	Morphology of Photopolymerized End-Linked Poly(ethylene glycol) Hydrogels by Small-Angle X-ray Scattering. Macromolecules, 2010, 43, 6861-6870.	2.2	87
167	Vertical confinement and interface effects on the microstructure and charge transport of P3HT thin films. Journal of Polymer Science, Part B: Polymer Physics, 2013, 51, 611-620.	2.4	87
168	Direct Uniaxial Alignment of a Donor–Acceptor Semiconducting Polymer Using Single-Step Solution Shearing. ACS Applied Materials & Interfaces, 2016, 8, 9285-9296.	4.0	87
169	Ordering Effects in Benzo[1,2â€ <i>b</i> :4,5â€ <i>b</i> ′]difuranâ€thieno[3,4â€ <i>c</i> ]pyrroleâ€4,6â€dione P with >7% Solar Cell Efficiency. Advanced Materials, 2014, 26, 4357-4362.	Polymers 11.1	85
170	Interplay between Energetic and Kinetic Factors on the Ambient Stability of n-Channel Organic Transistors Based on Perylene Diimide Derivatives. Chemistry of Materials, 2009, 21, 5508-5518.	3.2	84
171	Thiophene-rich fused-aromatic thienopyrazine acceptor for donor–acceptor low band-gap polymers for OTFT and polymer solar cell applications. Journal of Materials Chemistry, 2010, 20, 5823.	6.7	84
172	In situ measurement of power conversion efficiency and molecular ordering during thermal annealing in P3HT:PCBM bulk heterojunction solar cells. Journal of Materials Chemistry, 2011, 21, 15224.	6.7	84
173	Electrochemical ion insertion from the atomic to the device scale. Nature Reviews Materials, 2021, 6, 847-867.	23.3	84
174	Origin of low-friction behavior in graphite investigated by surface x-ray diffraction. Applied Physics Letters, 2004, 84, 4702-4704.	1.5	83
175	A Supramolecular Complex in Smallâ€Molecule Solar Cells based on Contorted Aromatic Molecules. Angewandte Chemie - International Edition, 2012, 51, 8594-8597.	7.2	82
176	Inverse design approach to hole doping in ternary oxides: Enhancing <mml:math xmlns:mml="http://www.w3.org/1998/Math/MathML" display="inline"&gt;<mml:mi>p</mml:mi>-type conductivity in cobalt oxide spinels. Physical Review B, 2011, 84, .</mml:math 	1.1	81
177	Effects of Odd–Even Side Chain Length of Alkyl-Substituted Diphenylbithiophenes on First Monolayer Thin Film Packing Structure. Journal of the American Chemical Society, 2013, 135, 11006-11014.	6.6	81
178	Acoustic phonon lifetimes limit thermal transport in methylammonium lead iodide. Proceedings of the National Academy of Sciences of the United States of America, 2018, 115, 11905-11910.	3.3	81
179	Observation of the effect of refraction on x rays diffracted in a grazing-incidence asymmetric Bragg geometry. Physical Review B, 1989, 39, 7963-7966.	1.1	80
180	Taming Charge Transport in Semiconducting Polymers with Branched Alkyl Side Chains. Advanced Functional Materials, 2017, 27, 1701973.	7.8	80

#	Article	IF	CITATIONS
181	Laser-Synthesized Epitaxial Graphene. ACS Nano, 2010, 4, 7524-7530.	7.3	79
182	Electron mean free path of tungsten and the electrical resistivity of epitaxial (110) tungsten films. Physical Review B, 2012, 86, .	1.1	79
183	Comparison of the Morphology Development of Polymer–Fullerene and Polymer–Polymer Solar Cells during Solutionâ€Shearing Blade Coating. Advanced Energy Materials, 2016, 6, 1601225.	10.2	79
184	Two-dimensional compressibility of electrochemically adsorbed lead on silver (111). Physical Review B, 1988, 38, 10962-10965.	1.1	78
185	Giant magnetoresistance and Co-cluster structure in phase-separated Co-Cu granular alloys. Physical Review B, 1993, 48, 16810-16813.	1.1	78
186	Particle size effect of hydrogen-induced lattice expansion of palladium nanoclusters. Physical Review B, 2008, 78, .	1.1	78
187	Structural Characterization of Vapor-Deposited Glasses of an Organic Hole Transport Material with X-ray Scattering. Chemistry of Materials, 2015, 27, 3341-3348.	3.2	78
188	10 Gbit/in.2 longitudinal media on a glass substrate (invited). Journal of Applied Physics, 1999, 85, 4286-4291.	1.1	77
189	Mechanistic Studies on Sintering of Silver Nanoparticles. Chemistry of Materials, 2011, 23, 4634-4640.	3.2	77
190	Effects of Confinement on Microstructure and Charge Transport in High Performance Semicrystalline Polymer Semiconductors. Advanced Functional Materials, 2013, 23, 2091-2098.	7.8	77
191	Morphological Origin of Charge Transport Anisotropy in Aligned Polythiophene Thin Films. Advanced Functional Materials, 2014, 24, 3422-3431.	7.8	77
192	Transformation from crystalline precursor to perovskite in PbCl2-derived MAPbI3. Nature Communications, 2018, 9, 3458.	5.8	77
193	Pore size distributions in nanoporous methyl silsesquioxane films as determined by small angle x-ray scattering. Applied Physics Letters, 2002, 81, 2232-2234.	1.5	76
194	Solid‣tate Supramolecular Organization of Polythiophene Chains Containing Thienothiophene Units. Advanced Materials, 2009, 21, 1193-1198.	11.1	76
195	Effect of Backbone Regioregularity on the Structure and Orientation of a Donor–Acceptor Semiconducting Copolymer. Macromolecules, 2014, 47, 1403-1410.	2.2	76
196	NASICON Na <sub>3</sub> V <sub>2</sub> (PO <sub>4</sub> ) <sub>3</sub> Enables Quasi-Two-Stage Na <sup>+</sup> and Zn <sup>2+</sup> Intercalation for Multivalent Zinc Batteries. Chemistry of Materials, 2020, 32, 3028-3035.	3.2	75
197	Beyond Local Solvation Structure: Nanometric Aggregates in Battery Electrolytes and Their Effect on Electrolyte Properties. ACS Energy Letters, 2022, 7, 461-470.	8.8	75
198	Correlating the microstructure of thin films of poly[5,5-bis(3-dodecyl-2-thienyl)-2,2-bithiophene] with charge transport: Effect of dielectric surface energy and thermal annealing. Physical Review B, 2008, 78, .	1.1	74

#	Article	IF	CITATIONS
199	Photovoltaic Universal Joints: Ballâ€andâ€Socket Interfaces in Molecular Photovoltaic Cells. ChemPhysChem, 2010, 11, 799-803.	1.0	74
200	Comparison of the Photovoltaic Characteristics and Nanostructure of Fullerenes Blended with Conjugated Polymers with Siloxane-Terminated and Branched Aliphatic Side Chains. Chemistry of Materials, 2013, 25, 431-440.	3.2	74
201	Underpotentially deposited thallium on silver (111) byin situsurface x-ray scattering. Physical Review B, 1992, 45, 9362-9374.	1.1	73
202	Measurements of carbon thin films using xâ€ray reflectivity. Journal of Applied Physics, 1989, 66, 1861-1863.	1.1	72
203	Magnetic anisotropy and microstructure in molecular beam epitaxial FePt (110)/MgO (110). Journal of Applied Physics, 1998, 84, 934-939.	1.1	72
204	Molecular design for improved photovoltaic efficiency: band gap and absorption coefficient engineering. Journal of Materials Chemistry, 2009, 19, 7195.	6.7	72
205	Can Polymorphism be Used to form Branched Metal Nanostructures?. Advanced Materials, 2013, 25, 1552-1556.	11.1	72
206	Size and composition distribution dynamics of alloy nanoparticle electrocatalysts probed by anomalous small angle X-ray scattering (ASAXS). Faraday Discussions, 2008, 140, 283-296.	1.6	71
207	The phase behavior of a polymerâ€fullerene bulk heterojunction system that contains bimolecular crystals. Journal of Polymer Science, Part B: Polymer Physics, 2011, 49, 499-503.	2.4	71
208	Emerging X-ray imaging technologies for energy materials. Materials Today, 2020, 34, 132-147.	8.3	70
209	All-Polymer Solar Cells Employing Non-Halogenated Solvent and Additive. Chemistry of Materials, 2016, 28, 5037-5042.	3.2	69
210	Small-Molecule Thiophene-C <sub>60</sub> Dyads As Compatibilizers in Inverted Polymer Solar Cells. Chemistry of Materials, 2010, 22, 5762-5773.	3.2	68
211	Effect of Surfactant Concentration and Aggregation on the Growth Kinetics of Nickel Nanoparticles. Journal of Physical Chemistry C, 2013, 117, 16709-16718.	1.5	68
212	Controlling the Microstructure of Solution-Processable Small Molecules in Thin-Film Transistors through Substrate Chemistry. Chemistry of Materials, 2011, 23, 1194-1203.	3.2	67
213	3,4-Disubstituted Polyalkylthiophenes for High-Performance Thin-Film Transistors and Photovoltaics. Journal of the American Chemical Society, 2011, 133, 16722-16725.	6.6	67
214	Surface x-ray-scattering measurements of the substrate-induced spatial modulation of an incommensurate adsorbed monolayer. Physical Review B, 1990, 42, 5594-5603.	1.1	66
215	Effects of the surface roughness of plastic-compatible inorganic dielectrics on polymeric thin film transistors. Applied Physics Letters, 2007, 90, 233508.	1.5	66
216	Mechanism of Crystallization and Implications for Charge Transport in Poly(3â€ethylhexylthiophene) Thin Films. Advanced Functional Materials, 2014, 24, 4515-4521.	7.8	66

#	Article	IF	CITATIONS
217	Crystallizationâ€Induced Phase Separation in Solutionâ€Processed Small Molecule Bulk Heterojunction Organic Solar Cells. Advanced Functional Materials, 2014, 24, 3543-3550.	7.8	66
218	In Situ Study of Silicon Electrode Lithiation with X-ray Reflectivity. Nano Letters, 2016, 16, 7394-7401.	4.5	66
219	General Post-annealing Method Enables High-Efficiency Two-Dimensional Perovskite Solar Cells. ACS Applied Materials & Interfaces, 2018, 10, 33187-33197.	4.0	66
220	Thin Film Structure of Tetraceno[2,3- <i>b</i> ]thiophene Characterized by Grazing Incidence X-ray Scattering and Near-Edge X-ray Absorption Fine Structure Analysis. Journal of the American Chemical Society, 2008, 130, 3502-3508.	6.6	65
221	Dealloying of Cu <sub>3</sub> Pt (111) Studied by Surface X-ray Scattering. Journal of Physical Chemistry C, 2011, 115, 9074-9080.	1.5	65
222	Ultrahigh Mobility in an Organic Semiconductor by Vertical Chain Alignment. Advanced Materials, 2016, 28, 2359-2366.	11.1	65
223	Nonâ€Conjugated Flexible Linkers in Semiconducting Polymers: A Pathway to Improved Processability without Compromising Device Performance. Advanced Electronic Materials, 2016, 2, 1600104.	2.6	65
224	Higher Mobility and Carrier Lifetimes in Solutionâ€Processable Smallâ€Molecule Ternary Solar Cells with 11% Efficiency. Advanced Energy Materials, 2019, 9, 1802836.	10.2	65
225	Subsurface Cooling Rates and Microstructural Response during Laser Based Metal Additive Manufacturing. Scientific Reports, 2020, 10, 1981.	1.6	64
226	Structural and Rheological Properties of Meibomian Lipid. , 2013, 54, 2720.		63
227	Carrier Transport and Recombination in Efficient "Allâ€Smallâ€Molecule―Solar Cells with the Nonfullerene Acceptor IDTBR. Advanced Energy Materials, 2018, 8, 1800264.	10.2	63
228	Low-energy electron diffraction study of molecular oxygen physisorbed on graphite. Physical Review B, 1987, 36, 1248-1258.	1.1	62
229	Influence of Surfactant Structure on Reverse Micelle Size and Charge for Nonpolar Electrophoretic Inks. Langmuir, 2011, 27, 11845-11851.	1.6	62
230	Correlating photovoltaic properties of a PTB7-Th:PC <sub>71</sub> BM blend to photophysics and microstructure as a function of thermal annealing. Journal of Materials Chemistry A, 2017, 5, 14646-14657.	5.2	61
231	In Situ Observation of Strain Development and Porosity Evolution in Nanoporous Gold Foils. Advanced Functional Materials, 2011, 21, 3938-3946.	7.8	60
232	Zone-Refinement Effect in Small Moleculeâ^'Polymer Blend Semiconductors for Organic Thin-Film Transistors. Journal of the American Chemical Society, 2011, 133, 412-415.	6.6	59
233	Tuning the Morphology of Solution-Sheared P3HT:PCBM Films. ACS Applied Materials & Interfaces, 2016, 8, 1742-1751.	4.0	59
234	Giant Magnetoresistance in As-Grown Epitaxial Films of Phase-Separated Co-Cu and Co-Ag. Europhysics Letters, 1993, 22, 455-462.	0.7	58

#	Article	IF	CITATIONS
235	The Role of Solvent Additive Processing in High Performance Small Molecule Solar Cells. Chemistry of Materials, 2014, 26, 6531-6541.	3.2	58
236	Tuning the bandgap of Cs <sub>2</sub> AgBiBr <sub>6</sub> through dilute tin alloying. Chemical Science, 2019, 10, 10620-10628.	3.7	58
237	Quantification of heterogeneous, irreversible lithium plating in extreme fast charging of lithium-ion batteries. Energy and Environmental Science, 2021, 14, 4979-4988.	15.6	58
238	Rotational epitaxy of a nontriangular structure: Thel̃´phase of oxygen physisorbed on graphite. Physical Review B, 1983, 27, 6413-6417.	1.1	57
239	In situ surface x-ray scattering measurements of electrochemically deposited bismuth on silver(111): structure, compressibility, and comparison with ex situ low-energy electron diffraction measurements. Langmuir, 1991, 7, 796-802.	1.6	57
240	Sequentially solution-processed, nanostructured polymer photovoltaics using selective solvents. Energy and Environmental Science, 2014, 7, 1103.	15.6	56
241	High-fraction brookite films from amorphous precursors. Scientific Reports, 2017, 7, 15232.	1.6	56
242	Growth temperature dependence of magnetoresistance in Co/Cu(111) wedged superlattices. Physical Review B, 1993, 47, 8721-8733.	1.1	55
243	Timeâ€Resolved Structural Kinetics of an Organic Mixed Ionic–Electronic Conductor. Advanced Materials, 2020, 32, e2003404.	11.1	55
244	Tuning the Morphology of All-Polymer OPVs through Altering Polymer–Solvent Interactions. Chemistry of Materials, 2014, 26, 5020-5027.	3.2	54
245	Xâ€ray reflectivity on perfluoropolyether polymer molecules on amorphous carbon. Journal of Chemical Physics, 1990, 92, 3781-3793.	1.2	53
246	Controlling the Texture and Crystallinity of Evaporated Lead Phthalocyanine Thin Films for Near-Infrared Sensitive Solar Cells. ACS Applied Materials & Interfaces, 2013, 5, 8505-8515.	4.0	53
247	Dopant activation in Sn-doped Ga2O3 investigated by X-ray absorption spectroscopy. Applied Physics Letters, 2015, 107, .	1.5	53
248	Ultrafast Electron Transfer at Organic Semiconductor Interfaces: Importance of Molecular Orientation. Journal of Physical Chemistry Letters, 2015, 6, 6-12.	2.1	52
249	Monitoring a Silent Phase Transition in CH <sub>3</sub> NH <sub>3</sub> PbI <sub>3</sub> Solar Cells via <i>Operando</i> X-ray Diffraction. ACS Energy Letters, 2016, 1, 1007-1012.	8.8	52
250	Water-in-Salt LiTFSI Aqueous Electrolytes. 1. Liquid Structure from Combined Molecular Dynamics Simulation and Experimental Studies. Journal of Physical Chemistry B, 2021, 125, 4501-4513.	1.2	52
251	High efficiency amine functionalization of cycloolefin polymer surfaces for biodiagnostics. Journal of Materials Chemistry, 2010, 20, 4116.	6.7	51
252	Temperature-Induced Transitions in the Structure and Interfacial Rheology of Human Meibum. Biophysical Journal, 2012, 102, 369-376.	0.2	51

#	Article	IF	CITATIONS
253	Storage Capacity and Cycling Stability in Ge Anodes: Relationship of Anode Structure and Cycling Rate. Advanced Energy Materials, 2015, 5, 1500599.	10.2	51
254	Coverage effects on the magnetism ofFeâ^•MgO(001)ultrathin films. Physical Review B, 2005, 71, .	1.1	50
255	Dealloyed PdCu3 thin film electrocatalysts for oxygen reduction reaction. Journal of Power Sources, 2013, 222, 169-176.	4.0	50
256	Humidity-Induced Photoluminescence Hysteresis in Variable Cs/Br Ratio Hybrid Perovskites. Journal of Physical Chemistry Letters, 2018, 9, 3463-3469.	2.1	50
257	Cross-Linked Ultrathin Polyurea Films via Molecular Layer Deposition. Macromolecules, 2013, 46, 5638-5643.	2.2	49
258	Origin of Anisotropic Molecular Packing in Vapor-Deposited Alq3 Glasses. Journal of Physical Chemistry Letters, 2019, 10, 164-170.	2.1	49
259	Heterogeneous Behavior of Lithium Plating during Extreme Fast Charging. Cell Reports Physical Science, 2020, 1, 100114.	2.8	49
260	Low-energy electron diffraction determination of the structure of thel¶phase of oxygen physisorbed on graphite. Physical Review B, 1984, 30, 1115-1118.	1.1	48
261	Thickness Measurements of Thin Perfluoropolyether Polymer Films on Silicon and Amorphous-Hydrogenated Carbon with X-Ray Reflectivity, ESCA and Optical Ellipsometry. Journal of Colloid and Interface Science, 2000, 225, 219-226.	5.0	47
262	Measuring Domain Sizes and Compositional Heterogeneities in P3HTâ€PCBM Bulk Heterojunction Thin Films with <sup>1</sup> H Spin Diffusion NMR Spectroscopy. Advanced Functional Materials, 2012, 22, 1255-1266.	7.8	47
263	Rapid fabrication of a novel Sn–Ge alloy: structure–property relationship and its enhanced lithium storage properties. Journal of Materials Chemistry A, 2013, 1, 14577.	5.2	47
264	Electric Field Tuning Molecular Packing and Electrical Properties of Solution‧hearing Coated Organic Semiconducting Thin Films. Advanced Functional Materials, 2017, 27, 1605503.	7.8	47
265	Thermal annealing study of exchangeâ€biased NiFeâ€FeMn films. Journal of Applied Physics, 1991, 70, 6227-6229.	1.1	46
266	Effects of stacking faults on magnetic viscosity in thin film magnetic recording media. Journal of Applied Physics, 1999, 85, 2775-2781.	1.1	46
267	A Quantitative Correlation between the Mobility and Crystallinity of Photo-Cross-Linkable P3HT. Macromolecules, 2012, 45, 3057-3062.	2.2	46
268	Novel phase diagram behavior and materials design in heterostructural semiconductor alloys. Science Advances, 2017, 3, e1700270.	4.7	46
269	The nanoscale structure of the electrolyte–metal oxide interface. Energy and Environmental Science, 2018, 11, 594-602.	15.6	46
270	Reversible Soft-Contact Lamination and Delamination for Non-Invasive Fabrication and Characterization of Bulk-Heterojunction and Bilayer Organic Solar Cells. Chemistry of Materials, 2010, 22, 4931-4938.	3.2	45

#	Article	IF	CITATIONS
271	Laserâ€Induced Keyhole Defect Dynamics during Metal Additive Manufacturing. Advanced Engineering Materials, 2019, 21, 1900455.	1.6	45
272	Water or Anion? Uncovering the Zn <sup>2+</sup> Solvation Environment in Mixed Zn(TFSI) <sub>2</sub> and LiTFSI Water-in-Salt Electrolytes. ACS Energy Letters, 2021, 6, 3458-3463.	8.8	45
273	Structural and magnetic model of self-assembled FePt nanoparticle arrays. Journal of Applied Physics, 2004, 96, 1197-1201.	1.1	44
274	A simple droplet pinning method for polymer film deposition for measuring charge transport in a thin film transistor. Organic Electronics, 2012, 13, 2450-2460.	1.4	43
275	Use of a commercially available nucleating agent to control the morphological development of solution-processed small molecule bulk heterojunction organic solar cells. Journal of Materials Chemistry A, 2014, 2, 15717-15721.	5.2	43
276	Mixed Domains Enhance Charge Generation and Extraction in Bulkâ€Heterojunction Solar Cells with Smallâ€Molecule Donors. Advanced Energy Materials, 2018, 8, 1702941.	10.2	43
277	Concentration and velocity profiles in a polymeric lithium-ion battery electrolyte. Energy and Environmental Science, 2020, 13, 4312-4321.	15.6	43
278	Crystalline Structure in Thin Films of DEHâ^'PPV Homopolymer and PPV-b-PI Rodâ^'Coil Block Copolymers. Macromolecules, 2008, 41, 58-66.	2.2	42
279	Influence of substrate on crystallization in polythiophene/fullerene blends. Solar Energy Materials and Solar Cells, 2011, 95, 1375-1381.	3.0	42
280	Molecular Structure of Interfacial Human Meibum Films. Langmuir, 2012, 28, 11858-11865.	1.6	42
281	Fluoroethylene Carbonate Induces Ordered Electrolyte Interface on Silicon and Sapphire Surfaces as Revealed by Sum Frequency Generation Vibrational Spectroscopy and X-ray Reflectivity. Nano Letters, 2018, 18, 2105-2111.	4.5	42
282	Donor Conjugated Polymers with Polar Side Chain Groups: The Role of Dielectric Constant and Energetic Disorder on Photovoltaic Performance. Advanced Functional Materials, 2018, 28, 1803418.	7.8	42
283	Preferred crystallographic orientation of cellulose in plant primary cell walls. Nature Communications, 2020, 11, 4720.	5.8	41
284	Agglomeration and sintering in annealed FePt nanoparticle assemblies studied by small angle neutron scattering and x-ray diffraction. Physical Review B, 2005, 72, .	1.1	40
285	Strain development in nanoporous metallic foils formed by dealloying. Applied Physics Letters, 2008, 92, .	1.5	40
286	Pâ€Type Transparent Cuâ€Alloyed ZnS Deposited at Room Temperature. Advanced Electronic Materials, 2016, 2, 1500396.	2.6	40
287	Inducing Molecular Aggregation of Polymer Semiconductors in a Secondary Insulating Polymer Matrix to Enhance Charge Transport. Chemistry of Materials, 2020, 32, 897-905.	3.2	40
288	Thickness dependence of exchange bias and structure in MnPt and MnNi spin valves. Applied Physics Letters, 2002, 81, 4565-4567.	1.5	39

#	Article	IF	CITATIONS
289	Tuning Contact Recombination and Open-Circuit Voltage in Polymer Solar Cells via Self-Assembled Monolayer Adsorption at the Organic–Metal Oxide Interface. Journal of Physical Chemistry C, 2013, 117, 20474-20484.	1.5	39
290	The Atomic Scale Electrochemical Lithiation and Delithiation Process of Silicon. Advanced Materials Interfaces, 2017, 4, 1700771.	1.9	39
291	Every Atom Counts: Elucidating the Fundamental Impact of Structural Change in Conjugated Polymers for Organic Photovoltaics. Chemistry of Materials, 2018, 30, 2995-3009.	3.2	39
292	Impact of Processing on Structural and Compositional Evolution in Mixed Metal Halide Perovskites during Film Formation. Advanced Functional Materials, 2020, 30, 2001752.	7.8	39
293	Toward Unraveling the Origin of Lithium Fluoride in the Solid Electrolyte Interphase. Chemistry of Materials, 2021, 33, 7315-7336.	3.2	39
294	Solutionâ€Processed Nanostructured Benzoporphyrin with Polycarbonate Binder for Photovoltaics. Advanced Materials, 2011, 23, 2289-2293.	11.1	38
295	Impact of Polymer Side Chain Modification on OPV Morphology and Performance. Chemistry of Materials, 2018, 30, 7872-7884.	3.2	38
296	Sulfur-Donor Solvents Strongly Coordinate Pb <sup>2+</sup> in Hybrid Organic–Inorganic Perovskite Precursor Solutions. Journal of Physical Chemistry C, 2020, 124, 14496-14502.	1.5	38
297	Morphological, Chemical, and Electronic Changes of the Conjugated Polymer PTB7 with Thermal Annealing. IScience, 2018, 2, 182-192.	1.9	37
298	Robust and Stretchable Polymer Semiconducting Networks: From Film Microstructure to Macroscopic Device Performance. Chemistry of Materials, 2019, 31, 6530-6539.	3.2	37
299	Dependence of Crystallite Formation and Preferential Backbone Orientations on the Side Chain Pattern in PBDTTPD Polymers. ACS Applied Materials & Interfaces, 2014, 6, 19477-19481.	4.0	36
300	Microstructure of Oligofluorene Asymmetric Derivatives in Organic Thin Film Transistors. Chemistry of Materials, 2008, 20, 2763-2772.	3.2	35
301	Self-Doping and Electrical Conductivity in Spinel Oxides: Experimental Validation of Doping Rules. Chemistry of Materials, 2014, 26, 1867-1873.	3.2	35
302	Compact Roll-to-Roll Coater for in Situ X-ray Diffraction Characterization of Organic Electronics Printing. ACS Applied Materials & Interfaces, 2016, 8, 1687-1694.	4.0	35
303	Radiative Thermal Annealing/in Situ X-ray Diffraction Study of Methylammonium Lead Triiodide: Effect of Antisolvent, Humidity, Annealing Temperature Profile, and Film Substrates. Chemistry of Materials, 2017, 29, 5931-5941.	3.2	35
304	Copper(I)-Based Highly Emissive All-Inorganic Rare-Earth Halide Clusters. Matter, 2019, 1, 180-191.	5.0	35
305	X-ray absorption and diffraction studies of thin polymer/FePt nanoparticle assemblies. Journal of Applied Physics, 2003, 93, 6299-6304.	1.1	34
306	Stoichiometry–anisotropy connections in epitaxial L10 FePt(001) films. Journal of Applied Physics, 2004, 95, 7501-7503.	1.1	34

#	Article	IF	CITATIONS
307	Silicide formation and particle size growth in high-temperature-annealed, self-assembled FePt nanoparticles. Journal of Applied Physics, 2004, 95, 6738-6740.	1.1	34
308	Fabrication of organic semiconductor crystalline thin films and crystals from solution by confined crystallization. Organic Electronics, 2012, 13, 235-243.	1.4	34
309	Negative-pressure polymorphs made by heterostructural alloying. Science Advances, 2018, 4, eaaq1442.	4.7	34
310	FA <sub><i>x</i></sub> Cs <sub>1–<i>x</i></sub> PbI <sub>3</sub> Nanocrystals: Tuning Crystal Symmetry by A-Site Cation Composition. ACS Energy Letters, 2020, 5, 2475-2482.	8.8	34
311	Atomic structure at electrode interfaces. Synchrotron Radiation News, 1993, 6, 28-33.	0.2	33
312	X-ray studies of magnetic nanoparticle assemblies. Journal of Applied Physics, 2003, 93, 7343-7345.	1.1	33
313	Vapor-Deposited Glass Structure Determined by Deposition Rate–Substrate Temperature Superposition Principle. Journal of Physical Chemistry Letters, 2019, 10, 3536-3542.	2.1	33
314	Advanced Characterization in Clean Water Technologies. Joule, 2020, 4, 1637-1659.	11.7	33
315	Stable solvent for solution-based electrical doping of semiconducting polymer films and its application to organic solar cells. Energy and Environmental Science, 2018, 11, 2216-2224.	15.6	32
316	Zn <sub>2</sub> SbN <sub>3</sub> : growth and characterization of a metastable photoactive semiconductor. Materials Horizons, 2019, 6, 1669-1674.	6.4	32
317	The Role of Metal Substitution in Tuning Anion Redox in Sodium Metal Layered Oxides Revealed by Xâ€Ray Spectroscopy and Theory. Angewandte Chemie - International Edition, 2021, 60, 10880-10887.	7.2	32
318	Achieving High Thermoelectric Performance and Metallic Transport in Solvent‧heared PEDOT:PSS. Advanced Electronic Materials, 2021, 7, 2001190.	2.6	32
319	Characterization of heterogeneity in the Heletz sandstone from core to pore scale and quantification of its impact on multi-phase flow. International Journal of Greenhouse Gas Control, 2016, 48, 69-83.	2.3	31
320	Near Surface Structure of Solvent-free Processed Polyimide Thin Film. Langmuir, 1996, 12, 2802-2806.	1.6	30
321	Pressure-induced quenching of the charge-density-wave state in rare-earth tritellurides observed by x-ray diffraction. Physical Review B, 2009, 79, .	1.1	30
322	Side chain engineering of fused aromatic thienopyrazine based low band-gap polymers for enhanced charge carrier mobility. Journal of Materials Chemistry, 2011, 21, 1537-1543.	6.7	30
323	Highly Organized Smectic-like Packing in Vapor-Deposited Glasses of a Liquid Crystal. Chemistry of Materials, 2017, 29, 849-858.	3.2	30
324	Vapor deposition of a nonmesogen prepares highly structured organic glasses. Proceedings of the National Academy of Sciences of the United States of America, 2019, 116, 21421-21426.	3.3	30

#	Article	IF	CITATIONS
325	Structural depth profiling of iron oxide thin films using grazing incidence asymmetric Bragg xâ€ray diffraction. Journal of Applied Physics, 1989, 65, 4763-4768.	1.1	29
326	Solution-Processable α,ω-Distyryl Oligothiophene Semiconductors with Enhanced Environmental Stability. Chemistry of Materials, 2009, 21, 1927-1938.	3.2	29
327	In situ X-ray-based imaging of nano materials. Current Opinion in Chemical Engineering, 2016, 12, 14-21.	3.8	29
328	Voltage-Controlled Interfacial Layering in an Ionic Liquid on SrTiO <sub>3</sub> . ACS Nano, 2016, 10, 4565-4569.	7.3	29
329	Operando Spectroscopic Microscopy of LiCoO2 Cathodes Outside Standard Operating Potentials. Electrochimica Acta, 2017, 247, 977-982.	2.6	29
330	Zinc Blende Magnesium Sulfide in Rechargeable Magnesium-Sulfur Batteries. Chemistry of Materials, 2018, 30, 6318-6324.	3.2	29
331	Coulombically-stabilized oxygen hole polarons enable fully reversible oxygen redox. Energy and Environmental Science, 2021, 14, 4858-4867.	15.6	29
332	Synthesis and Characterization of K <sub>8â~<i>x</i></sub> (H <sub>2</sub> ) <sub><i>y</i></sub> Si <sub>46</sub> . Inorganic Chemistry, 2010, 49, 815-822.	1.9	28
333	Identifying and managing radiation damage during in situ transmission x-ray microscopy of Li-ion batteries. Proceedings of SPIE, 2013, , .	0.8	28
334	Impact of Hole Transport Layer Surface Properties on the Morphology of a Polymerâ€Fullerene Bulk Heterojunction. Advanced Energy Materials, 2014, 4, 1301879.	10.2	28
335	Interfacial Speciation Determines Interfacial Chemistry: Xâ€rayâ€Induced Lithium Fluoride Formation from Waterâ€inâ€salt Electrolytes on Solid Surfaces. Angewandte Chemie - International Edition, 2020, 59, 23180-23187.	7.2	28
336	The Crystalline Structure of Copper Phthalocyanine Films on ZnO(11Ì00). Journal of the American Chemical Society, 2012, 134, 14302-14305.	6.6	27
337	Growth Trajectories and Coarsening Mechanisms of Metal Nanoparticle Electrocatalysts. ChemCatChem, 2012, 4, 766-770.	1.8	27
338	Ultrathin Body Poly(3-hexylthiophene) Transistors with Improved Short-Channel Performance. ACS Applied Materials & Interfaces, 2013, 5, 2342-2346.	4.0	27
339	Spectromicroscopy and coherent diffraction imaging: focus on energy materials applications. Journal of Synchrotron Radiation, 2014, 21, 1019-1030.	1.0	27
340	Growth of Highly Strained CeO <sub>2</sub> Ultrathin Films. ACS Nano, 2016, 10, 9938-9947.	7.3	27
341	Enhancing Molecular Alignment and Charge Transport of Solutionâ€Sheared Semiconducting Polymer Films by the Electricalâ€Blade Effect. Advanced Electronic Materials, 2018, 4, 1800110.	2.6	27
342	Mechanism of Additive-Assisted Room-Temperature Processing of Metal Halide Perovskite Thin Films. ACS Applied Materials & Interfaces, 2021, 13, 13212-13225.	4.0	27

#	Article	IF	CITATIONS
343	Influence of Annealing and Composition on the Crystal Structure of Mixed-Halide, Ruddlesden–Popper Perovskites. Chemistry of Materials, 2022, 34, 3109-3122.	3.2	27
344	Temperature dependent chemical ordering in FePt(001) and FePt(110) films. Journal of Applied Physics, 2000, 87, 6956-6958.	1.1	26
345	Supercritical carbon dioxide extraction of porogens for the preparation of ultralow-dielectric-constant films. Applied Physics Letters, 2003, 82, 4328-4330.	1.5	26
346	Effect of Solvent Additives on the Solution Aggregation of Phenyl-C <sub>61</sub> –Butyl Acid Methyl Ester (PCBM). Chemistry of Materials, 2015, 27, 8261-8272.	3.2	26
347	Mechanism of Na <sup>+</sup> Insertion in Alkali Vanadates and Its Influence on Battery Performance. Advanced Energy Materials, 2016, 6, 1502336.	10.2	26
348	Understanding additive controlled lithium morphology in lithium metal batteries. Journal of Materials Chemistry A, 2020, 8, 16960-16972.	5.2	26
349	Degradation mechanisms in mixed-cation and mixed-halide Cs <sub>x</sub> FA <sub>1â^'x</sub> Pb(Br <sub>y</sub> Isub>1â^'y) <sub>3</sub> perovskite films under ambient conditions. Journal of Materials Chemistry A, 2020, 8, 9302-9312.	5.2	26
350	Clipped Random Wave Morphologies and the Analysis of the SAXS of an Ionomer Formed by Copolymerization of Tetrafluoroethylene and CF2â•€FO(CF2)4SO3H. Macromolecules, 2009, 42, 5774-5780.	2.2	25
351	Modified magnetic ground state in <mml:math <br="" xmlns:mml="http://www.w3.org/1998/Math/MathML">display="inline"&gt;<mml:mrow><mml:msub><mml:mrow><mml:mtext>NiMn</mml:mtext></mml:mrow><mml:mi Asymfiletsic.daRonenofist@fdfioffetry in spinels: Site occupancy in Co<mml:math< td=""><td>۱&gt;<b>2.₄</b>/mml</td><td>:m<b>മ5</b> </td></mml:math<></mml:mi </mml:msub></mml:mrow></mml:math>	۱> <b>2.₄</b> /mml	:m <b>മ5</b>
352	xmlns:mml="http://www.w3.org/1998/Math/MathML" display="inline"> <mml:msub><mml:mrow /&gt;<mml:mn>2</mml:mn></mml:mrow </mml:msub> ZnO <mml:math xmlns:mml="http://www.w3.org/1998/Math/MathML" display="inline"&gt;<mml:msub><mml:mrow /&gt;<mml:mn>4</mml:mn></mml:mrow </mml:msub>and Rh<mml:math xmlns:mml="http://www.w3.org/1998/Math/MathML" display="inline"&gt;<mml:msub><mml:mrow< td=""><td>1.1</td><td>25</td></mml:mrow<></mml:msub></mml:math </mml:math 	1.1	25
353	Substrate-Induced Variations of Molecular Packing, Dynamics, and Intermolecular Electronic Couplings in Pentacene Monolayers on the Amorphous Silica Dielectric. ACS Nano, 2014, 8, 690-700.	7.3	25
354	Vapor-Deposited Glasses with Long-Range Columnar Liquid Crystalline Order. Chemistry of Materials, 2017, 29, 9110-9119.	3.2	25
355	Shedding X-ray Light on the Interfacial Electrochemistry of Silicon Anodes for Li-Ion Batteries. Accounts of Chemical Research, 2019, 52, 2673-2683.	7.6	25
356	Cooling dynamics of two titanium alloys during laser powder bed fusion probed with in situ X-ray imaging and diffraction. Materials and Design, 2020, 195, 108987.	3.3	25
357	Toward quantifying capacity losses due to solid electrolyte interphase evolution in silicon thin film batteries. Journal of Chemical Physics, 2020, 152, 084702.	1.2	25
358	Instrumental effects on measurements of surface X-ray diffraction rods: resolution function and active sample area. Acta Crystallographica Section A: Foundations and Advances, 1993, 49, 624-642.	0.3	24
359	Structural properties of epitaxial SrHfO3 thin films on Si (001). Thin Solid Films, 2010, 518, S118-S122.	0.8	24
360	Chemical Annealing of Zinc Tetraphenylporphyrin Films: Effects on Film Morphology and Organic Photovoltaic Performance. Chemistry of Materials, 2012, 24, 2583-2591.	3.2	24

#	Article	IF	CITATIONS
361	Solution-Phase Conformation and Dynamics of Conjugated Isoindigo-Based Donor–Acceptor Polymer Single Chains. Journal of Physical Chemistry Letters, 2017, 8, 5479-5486.	2.1	24
362	Tuning Intra and Intermolecular Interactions for Balanced Hole and Electron Transport in Semiconducting Polymers. Chemistry of Materials, 2020, 32, 7338-7346.	3.2	24
363	Alloying a single and a double perovskite: a Cu <sup>+/2+</sup> mixed-valence layered halide perovskite with strong optical absorption. Chemical Science, 2021, 12, 8689-8697.	3.7	24
364	Structural effect of PtRu–WO3 alloy nanostructures on methanol electrooxidation. Electrochemistry Communications, 2006, 8, 359-363.	2.3	23
365	Thin Film Transistors Based on Alkylphenyl Quaterthiophenes:Â Structure and Electrical Transport Properties. Chemistry of Materials, 2007, 19, 1355-1361.	3.2	23
366	Insertion Mechanism of a Poly(ethylene oxide)-poly(butylene oxide) Block Copolymer into a DPPC Monolayer. Langmuir, 2011, 27, 11444-11450.	1.6	23
367	Tuning crystalline ordering by annealing and additives to study its effect on exciton diffusion in a polyalkylthiophene copolymer. Physical Chemistry Chemical Physics, 2017, 19, 12441-12451.	1.3	23
368	High-capacity thermochemical CO <sub>2</sub> dissociation using iron-poor ferrites. Energy and Environmental Science, 2020, 13, 592-600.	15.6	23
369	Mixing Matters: Nanoscale Heterogeneity and Stability in Metal Halide Perovskite Solar Cells. ACS Energy Letters, 2022, 7, 471-480.	8.8	23
370	Probing the effect of substrate heating during deposition of DCV4T:C60 blend layers for organic solar cells. Organic Electronics, 2012, 13, 623-631.	1.4	22
371	Synthesis, solidâ€state, and chargeâ€transport properties of conjugated polythiopheneâ€ <i>S</i> , <i>S</i> â€dioxides. Journal of Polymer Science, Part B: Polymer Physics, 2013, 51, 48-56.	2.4	22
372	Over What Length Scale Does an Inorganic Substrate Perturb the Structure of a Glassy Organic Semiconductor?. ACS Applied Materials & amp; Interfaces, 2020, 12, 26717-26726.	4.0	22
373	<i>GIWAXS-SIIRkit</i> : scattering intensity, indexing and refraction calculation toolkit for grazing-incidence wide-angle X-ray scattering of organic materials. Journal of Applied Crystallography, 2020, 53, 1108-1129.	1.9	22
374	Giant magnetoresistance at low fields in [(NixFe1â^'x)yAg1â^'y]/Ag multilayers prepared by molecularâ€beam epitaxy. Journal of Applied Physics, 1994, 76, 3688-3694.	1.1	21
375	Roughness of molecularly thin perfluoropolyether polymer films. Applied Physics Letters, 2000, 77, 3296-3298.	1.5	21
376	Templating Organosilicate Vitrification Using Unimolecular Self-Organizing Polymers: Evolution of Morphology and Nanoporosity Development with Network Formation. Advanced Materials, 2005, 17, 1031-1035.	11.1	21
377	Engineering epitaxial Î <sup>3</sup> -Al2O3 gate dielectric films on 4H-SiC. Journal of Applied Physics, 2007, 102, 104112.	1.1	21
378	Improved Efficiency in Poly(3-hexylthiophene)/Zinc Oxide Solar Cells via Lithium Incorporation. Journal of Physical Chemistry C, 2009, 113, 17608-17612.	1.5	21

#	Article	IF	CITATIONS
379	Two-Dimensional GIWAXS Reveals a Transient Crystal Phase in Solution-Processed Thermally Converted Tetrabenzoporphyrin. Journal of Physical Chemistry B, 2013, 117, 14557-14567.	1.2	21
380	Understanding the Impact of Oligomeric Polystyrene Side Chain Arrangement on the Allâ€Polymer Solar Cell Performance. Advanced Energy Materials, 2018, 8, 1701552.	10.2	21
381	Operando Spectromicroscopy of Sulfur Species in Lithium-Sulfur Batteries. Journal of the Electrochemical Society, 2018, 165, A6043-A6050.	1.3	21
382	Microstructural Evolution of the Thin Films of a Donor–Acceptor Semiconducting Polymer Deposited by Meniscus-Guided Coating. Macromolecules, 2018, 51, 4325-4340.	2.2	21
383	Bridging the thermodynamics and kinetics of temperature-induced morphology evolution in polymer/fullerene organic solar cell bulk heterojunction. Materials Horizons, 2021, 8, 1272-1285.	6.4	21
384	Nanoscale phase separation in Fe3O4(111) films on sapphire(0001) and phase stability of Fe3O4(001) films on MgO(001) grown by oxygen-plasma-assisted molecular beam epitaxy. Journal of Applied Physics, 2003, 93, 5626-5636.	1.1	20
385	Operando X-ray Studies of Crystalline Ge Anodes with Different Conductive Additives. Journal of Physical Chemistry C, 2015, 119, 22772-22777.	1.5	20
386	Extraction of pore-morphology and capillary pressure curves of porous media from synchrotron-based tomography data. Scientific Reports, 2015, 5, 10635.	1.6	20
387	Impact of the Crystallite Orientation Distribution on Exciton Transport in Donor–Acceptor Conjugated Polymers. ACS Applied Materials & Interfaces, 2015, 7, 28035-28041.	4.0	20
388	Synthesis of Poly(bisisoindigo) Using a Metal-Free Aldol Polymerization for Thin-Film Transistor Applications. ACS Applied Materials & Interfaces, 2020, 12, 14265-14271.	4.0	20
389	Compositional heterogeneity in Cs <sub><i>y</i></sub> FA <sub>1â<sup>^</sup><i>y</i></sub> Pb(Br <sub><i>x</i></sub> I <sub>1â<sup>^</sup><i>x</i></sub> ) <sub>3&lt; perovskite films and its impact on phase behavior. Energy and Environmental Science, 2021, 14, 6394-6405.</sub>	/sub> 15.6	20
390	Unraveling the Unconventional Order of a High-Mobility Indacenodithiophene–Benzothiadiazole Copolymer. ACS Macro Letters, 2021, 10, 1306-1314.	2.3	20
391	Comment on â€~ã€~Superstructures of Pb monolayers electrochemically deposited on Ag(111)''. Physical Review B, 1994, 49, 7793-7794.	1.1	19
392	X-Ray Probes for <i>In Situ</i> Studies of Interfaces. MRS Bulletin, 2010, 35, 504-513.	1.7	19
393	Synthesis of regioregular pentacene-containing conjugated polymers. Journal of Materials Chemistry, 2011, 21, 7078.	6.7	19
394	Behaviors of Fe, Zn, and Ga Substitution in CuInS <sub>2</sub> Nanoparticles Probed with Anomalous X-ray Diffraction. Chemistry of Materials, 2013, 25, 320-325.	3.2	19
395	Registration of the rotation axis in X-ray tomography. Journal of Synchrotron Radiation, 2015, 22, 452-457.	1.0	19
396	In situ probing of the crystallization kinetics of rr-P3HT on single layer graphene as a function of temperature. Physical Chemistry Chemical Physics, 2017, 19, 8496-8503.	1.3	19

#	Article	IF	CITATIONS
397	Using heterostructural alloying to tune the structure and properties of the thermoelectric Sn <sub>1â^'x</sub> Ca <sub>x</sub> Se. Journal of Materials Chemistry A, 2017, 5, 16873-16882.	5.2	19
398	Molecular Orientation for Vapor-Deposited Organic Glasses Follows Rate-Temperature Superposition: The Case of Posaconazole. Journal of Physical Chemistry B, 2020, 124, 2505-2513.	1.2	19
399	Modular construction of P3HT/PCBM planar-heterojunction solar cells by lamination allows elucidation of processing–structure–function relationships. Organic Electronics, 2011, 12, 1963-1972.	1.4	18
400	Role of Solution Structure in Self-Assembly of Conjugated Block Copolymer Thin Films. Macromolecules, 2016, 49, 8187-8197.	2.2	18
401	Exploring the influence of iron substitution in lithium rich layered oxides Li <sub>2</sub> Ru <sub>1â^'x</sub> Fe <sub>x</sub> O <sub>3</sub> : triggering the anionic redox reaction. Journal of Materials Chemistry A, 2017, 5, 14387-14396.	5.2	18
402	Synthesis of Polycrystalline Ruddlesden–Popper Organic Lead Halides and Their Growth Dynamics. Chemistry of Materials, 2019, 31, 9472-9479.	3.2	18
403	Melting of Magnesium Borohydride under High Hydrogen Pressure: Thermodynamic Stability and Effects of Nanoconfinement. Chemistry of Materials, 2020, 32, 5604-5615.	3.2	18
404	<i>In Situ</i> X-Ray-Diffraction Studies of Passive Oxide Films. MRS Bulletin, 1999, 24, 29-35.	1.7	17
405	High anisotropy CoPtCrB magnetic recording media. Journal of Applied Physics, 2003, 94, 4018-4023.	1.1	17
406	Pore Morphologies in Disordered Nanoporous Thin Films. Langmuir, 2004, 20, 1535-1538.	1.6	17
407	Effects of Thermal Annealing Upon the Nanomorphology of Poly(3â€hexylselenophene)â€₽CBM Blends. Macromolecular Rapid Communications, 2011, 32, 1454-1460.	2.0	17
408	Efficient Energy Sensitization of C <sub>60</sub> and Application to Organic Photovoltaics. Journal of the American Chemical Society, 2013, 135, 11920-11928.	6.6	17
409	Reduced crystallinity and enhanced charge transport by melt annealing of an organic semiconductor on single layer graphene. Journal of Materials Chemistry C, 2016, 4, 4143-4149.	2.7	17
410	Langmuir–Blodgett Thin Films of Diketopyrrolopyrrole-Based Amphiphiles. ACS Applied Materials & Interfaces, 2018, 10, 11995-12004.	4.0	17
411	Using Deposition Rate and Substrate Temperature to Manipulate Liquid Crystal-Like Order in a Vapor-Deposited Hexagonal Columnar Glass. Journal of Physical Chemistry B, 2021, 125, 2761-2770.	1.2	17
412	Quantification of Efficiency in Lithium Metal Negative Electrodes via Operando X-ray Diffraction. Chemistry of Materials, 2021, 33, 7537-7545.	3.2	17
413	Using <i>In Situ</i> High-Energy X-ray Diffraction to Quantify Electrode Behavior of Li-Ion Batteries from Extreme Fast Charging. ACS Applied Energy Materials, 2021, 4, 11590-11598.	2.5	17
414	Structure and epitaxy of anodic TiO2/Ti(110). Surface Science, 1992, 268, 57-72.	0.8	16

#	Article	IF	CITATIONS
415	5,11-Conjugation-extended low-bandgap anthradithiophene-containing polymer exhibiting enhanced thin-film order and field-effect mobility. Chemical Communications, 2012, 48, 7286.	2.2	16
416	Tuning domain size and crystallinity in isoindigo/PCBM organic solar cells via solution shearing. Organic Electronics, 2017, 40, 79-87.	1.4	16
417	Supercritical CO2extraction of porogen phase: An alternative route to nanoporous dielectrics. Journal of Materials Research, 2004, 19, 3224-3233.	1.2	15
418	Microstructural comparisons of ultrathin Cu films deposited by ion-beam and dc-magnetron sputtering. Journal of Applied Physics, 2005, 97, 093301.	1,1	15
419	Structural properties of epitaxial γ-Al2O3 (111) thin films on 4H-SiC (0001). Applied Physics Letters, 2007, 90, 061916.	1.5	15
420	Langmuir Monolayers of Straight-Chain and Branched Hexadecanol and Eicosanol Mixtures. Langmuir, 2008, 24, 14005-14014.	1.6	15
421	Square Grains in Asymmetric Rodâ^'Coil Block Copolymers. Langmuir, 2008, 24, 1604-1607.	1.6	15
422	Co3O4–Co2ZnO4 spinels: The case for a solid solution. Journal of Solid State Chemistry, 2012, 190, 143-149.	1.4	15
423	Dynamical Orientation of Large Molecules on Oxide Surfaces and its Implications for Dye-Sensitized Solar Cells. Chemistry of Materials, 2013, 25, 4354-4363.	3.2	15
424	Understanding the Selective Etching of Electrodeposited ZnO Nanorods. Langmuir, 2014, 30, 14079-14085.	1.6	15
425	Rapid thermal processing chamber for <i>in-situ</i> x-ray diffraction. Review of Scientific Instruments, 2015, 86, 013902. X-Ray Absorption Spectroscopy Study of Structure and Stability of Disordered	0.6	15
40.6	(Cu <inline-formula> <tex-math>\$_{f} Tj ETQq0 0 0 rgBT /Overlock 10 Tf 50 312 Td (2}\$<td>0</td><td>·</td></tex-math></inline-formula>	0	·
426	1-x}\$(ZnS) <inline-formula><tex-math>\$_{f</tex-math></inline-formula>	1.5	15
427	x}\$  Alloys. IEEE Journal of Photovoltaics, 2015, 5, 372-377. Influence of amorphous structure on polymorphism in vanadia. APL Materials, 2016, 4, .	2.2	15
428	Kinetic Versus Thermodynamic Orientational Preferences for a Series of Isomorphic Molecular Semiconductors. ACS Omega, 2018, 3, 10198-10204.	1.6	15
429	Acceptor Gradient Polymer Donors for Non-Fullerene Organic Solar Cells. Chemistry of Materials, 2019, 31, 9729-9741.	3.2	15
430	Spontaneous chemical ordering and exchange bias in epitaxial Mn0.52Pd0.48/Fe(001) bilayers prepared at room temperature. Applied Physics Letters, 2002, 80, 808-810.	1.5	14
431	Small-angle neutron scattering measurements of magnetic cluster sizes in magnetic recording disks. Applied Physics Letters, 2003, 82, 3050-3052.	1.5	14
432	Structure of oxidized bismuth nanoclusters. Acta Crystallographica Section B: Structural Science, 2007, 63, 569-576.	1.8	14

#	ARTICLE density wave formation in <mml:math <br="" xmlns:mml="http://www.w3.org/1998/Math/MathML">display="inline"&gt; <mml:mrow> <mml:msub> <mml:mi> R </mml:mi> &lt; mml:mi&gt; 2  2  </mml:msub> <mml:msub< th=""><th>IF</th><th>CITATIONS</th></mml:msub<></mml:mrow></mml:math>	IF	CITATIONS
433	mathvariant="normal">Te <mml:mn>5</mml:mn> ( <mml:math< th=""><th></th><th></th></mml:math<>		
434	Ty Impact of regioregularity on thin-film transistor and photovoltaic cell performances of pentacene-containing polymers. Journal of Materials Chemistry, 2012, 22, 4356.	6.7	14
435	Experimental Characterization of a Theoretically Designed Candidate p-Type Transparent Conducting Oxide: Li-Doped Cr <sub>2</sub> MnO <sub>4</sub> . Chemistry of Materials, 2014, 26, 4598-4604.	3.2	14
436	On twin density and resistivity of nanometric Cu thin films. Journal of Applied Physics, 2016, 120, .	1.1	14
437	Point defects in Cu 2 ZnSnSe 4 (CZTSe): Resonant Xâ€ray diffraction study of the lowâ€temperature order/disorder transition. Physica Status Solidi (B): Basic Research, 2017, 254, 1700156.	0.7	14
438	Generic packing motifs in vapor-deposited glasses of organic semiconductors. Soft Matter, 2019, 15, 7590-7595.	1.2	14
439	Controlling Polymer Morphology in Blade-Coated All-Polymer Solar Cells. Chemistry of Materials, 2021, 33, 5951-5961.	3.2	14
440	Highly Reversible Plating/Stripping of Porous Zinc Anodes for Multivalent Zinc Batteries. Journal of the Electrochemical Society, 2020, 167, 140520.	1.3	14
441	Elastic properties of chemically ordered Co3Pt thin films. Journal of Applied Physics, 2002, 91, 2737-2741.	1.1	13
442	Reticulated Organic Photovoltaics. Advanced Functional Materials, 2012, 22, 1167-1173.	7.8	13
443	Quantifying point defects in Cu2ZnSn(S,Se)4 thin films using resonant x-ray diffraction. Applied Physics Letters, 2016, 109, .	1.5	13
444	Direct in situ observation of ZnO nucleation and growth via transmission X-ray microscopy. Nanoscale, 2016, 8, 1849-1853.	2.8	13
445	Graphene induced electrical percolation enables more efficient charge transport at a hybrid organic semiconductor/graphene interface. Physical Chemistry Chemical Physics, 2018, 20, 4422-4428.	1.3	13
446	Augmenting n-Type Performance of Ambipolar Top-Contact Organic Thin-Film Transistors by Self-Generated Interlayers. Chemistry of Materials, 2019, 31, 7046-7053.	3.2	13
447	Selective brookite polymorph formation related to the amorphous precursor state in TiO2 thin films. Journal of Non-Crystalline Solids, 2019, 505, 109-114.	1.5	13
448	Test of the Dynamic-Domain and Critical Scattering Hypotheses in Cubic Methylammonium Lead Triiodide. Physical Review Letters, 2020, 125, .	2.9	13
449	Using resonant energy X-ray diffraction to extract chemical order parameters in ternary semiconductors. Journal of Materials Chemistry C, 2020, 8, 4350-4356.	2.7	13
450	Electrochemical and electrochromic properties of nanoworm-shaped Ta2O5–Pt thin-films. Electrochemistry Communications, 2005, 7, 151-155.	2.3	12

#	Article	IF	CITATIONS
451	In Situ Synchrotron X-ray Diffraction Experiments on Electrochemically Deposited ZnO Nanostructures. Journal of Physical Chemistry C, 2008, 112, 14863-14866.	1.5	12
452	In situ USAXS measurements of titania colloidal paint films during the drying process. Journal of Colloid and Interface Science, 2009, 336, 612-615.	5.0	12
453	Thermotropic Phase Transition of Benzodithiophene Copolymer Thin Films and Its Impact on Electrical and Photovoltaic Characteristics. Chemistry of Materials, 2015, 27, 1223-1232.	3.2	12
454	Li gradients for Li-rich cathodes. Nature Energy, 2019, 4, 1014-1015.	19.8	12
455	Analysis and Simulation of One-Dimensional Transport Models for Lithium Symmetric Cells. Journal of the Electrochemical Society, 2019, 166, A3806-A3819.	1.3	12
456	In Situ Characterization of Ferroelectric HfO <sub>2</sub> During Rapid Thermal Annealing. Physica Status Solidi - Rapid Research Letters, 2021, 15, 2000598.	1.2	12
457	Orientation-Dependent Distortion of Lamellae in a Block Copolymer Electrolyte under DC Polarization. Macromolecules, 2021, 54, 7808-7821.	2.2	12
458	Studies of Electrodes by in Situ X-Ray Scattering. , 1994, , 109-125.		12
459	Structure and Electrocatalysis of Sputtered RuPt Thin-Film Electrodes. Journal of Physical Chemistry B, 2005, 109, 12845-12849.	1.2	11
460	Simplified Models for Accelerated Structural Prediction of Conjugated Semiconducting Polymers. Journal of Physical Chemistry C, 2017, 121, 26528-26538.	1.5	11
461	Understanding the reactivity of CoCrMo-implant wear particles. Npj Materials Degradation, 2018, 2, .	2.6	11
462	Hydrogen Purification in Palladium-Based Membranes: An Operando X-ray Diffraction Study. Industrial & Engineering Chemistry Research, 2019, 58, 926-934.	1.8	11
463	Surface equilibration mechanism controls the molecular packing of glassy molecular semiconductors at organic interfaces. Proceedings of the National Academy of Sciences of the United States of America, 2021, 118, .	3.3	11
464	Scattering techniques for mixed donor–acceptor characterization in organic photovoltaics. Materials Horizons, 2022, 9, 43-60.	6.4	11
465	Reduction of resistivity in Cu thin films by partial oxidation: Microstructural mechanisms. Applied Physics Letters, 2004, 84, 2518-2520.	1.5	10
466	Influence of Interfacial Layer Between Nanoparticles and Polymeric Matrix on Viscoelastic Properties of Hydrogel Nanocomposites. Macromolecules, 2009, 42, 1331-1343.	2.2	10
467	Absence of Mixed Phase in Organic Photovoltaic Active Layers Facilitates Use of Green Solvent Processing. Journal of Physical Chemistry C, 2018, 122, 11136-11144.	1.5	10
468	Effect of Molecular Shape on the Properties of Non-Fullerene Acceptors: Contrasting Calamitic Versus 3D Design Principles. ACS Applied Energy Materials, 2018, 1, 6513-6523.	2.5	10

#	Article	IF	CITATIONS
469	Fullerene derivative induced morphology of bulk heterojunction blends: PIPCP:PC <sub>61</sub> BM. RSC Advances, 2019, 9, 4106-4112.	1.7	10
470	The Role of Metal Substitution in Tuning Anion Redox in Sodium Metal Layered Oxides Revealed by Xâ€Ray Spectroscopy and Theory. Angewandte Chemie, 2021, 133, 10975-10982.	1.6	10
471	X-ray diffraction from anodic TiO2 films: in situ and ex situ comparison of the Ti (0001) face. Surface Science, 1994, 302, 341-349.	0.8	9
472	Local Atomic Structure of Partially Ordered NiMn in NiMn/NiFe Exchange Coupled Layers:Â 1. XAFS Measurements and Structural Refinement. Journal of Physical Chemistry B, 2005, 109, 10406-10418.	1.2	9
473	Synchrotron x-ray diffraction measurements of strain in metallic nanoparticles with oxide shells. Journal Physics D: Applied Physics, 2010, 43, 075301.	1.3	9
474	SAXSMorph: a program for generating representative morphologies for two-phase materials from small-angle X-ray and neutron scattering data. Journal of Applied Crystallography, 2011, 44, 221-224.	1.9	9
475	Formation of Nanoscale Composites of Compound Semiconductors Driven by Charge Transfer. Nano Letters, 2016, 16, 5247-5254.	4.5	9
476	The effect of sub-oxide phases on the transparency of tin-doped gallium oxide. Applied Physics Letters, 2016, 109, .	1.5	9
477	Vanadium As a Potential Membrane Material for Carbon Capture: Effects of Minor Flue Gas Species. Environmental Science & Technology, 2017, 51, 11459-11467.	4.6	9
478	Triptycene as a Supramolecular Additive in PTB7:PCBM Blends and Its Influence on Photovoltaic Properties. ACS Applied Materials & Interfaces, 2018, 10, 24665-24678.	4.0	9
479	Interfacial Speciation Determines Interfacial Chemistry: Xâ€rayâ€Induced Lithium Fluoride Formation from Waterâ€inâ€salt Electrolytes on Solid Surfaces. Angewandte Chemie, 2020, 132, 23380-23387.	1.6	9
480	Combined Effects of Uniform Applied Pressure and Electrolyte Additives in Lithium-Metal Batteries. ACS Applied Energy Materials, 2022, 5, 8273-8281.	2.5	9
481	XRD., 1992, , 198-213.		8
482	Nonequilibrium 2-Hydroxyoctadecanoic Acid Monolayers: Effect of Electrolytes. Langmuir, 2011, 27, 4430-4438.	1.6	8
483	Swelling of Polymer Dielectric Thin Films for Organic-Transistor-Based Aqueous Sensing Applications. Chemistry of Materials, 2013, 25, 5018-5022.	3.2	8
484	Effects of aromatic regularity on the structure and conductivity of polyimideâ€poly(ethylene glycol) materials doped with ionic liquid. Journal of Polymer Science, Part B: Polymer Physics, 2015, 53, 509-521.	2.4	8
485	Unique Reversible Crystal-to-Crystal Phase Transition—Structural and Functional Properties of Fused Ladder Thienoarenes. Chemistry of Materials, 2017, 29, 7686-7696.	3.2	8
486	Improving molecular alignment and charge percolation in semiconducting polymer films with highly localized electronic states through tailored thermal annealing. Journal of Materials Chemistry C, 2021, 9, 15848-15857.	2.7	8

#	Article	IF	CITATIONS
487	Vapor deposition rate modifies anisotropic glassy structure of an anthracene-based organic semiconductor. Journal of Chemical Physics, 2022, 156, 014504.	1.2	8
488	Revealing temperature-dependent polymer aggregation in solution with small-angle X-ray scattering. Journal of Materials Chemistry A, 2022, 10, 2096-2104.	5.2	8
489	Conformal Pressure and Fast-Charging Li-Ion Batteries. Journal of the Electrochemical Society, 2022, 169, 040540.	1.3	8
490	Oxygen-enhanced IrMn spin valves deposited by ion-beam and magnetron sputtering. Journal of Applied Physics, 2001, 89, 6925-6927.	1.1	7
491	Organic Solar Cells: How X-ray Scattering Has Improved Our Understanding of Morphology. Synchrotron Radiation News, 2010, 23, 16-21.	0.2	7
492	Evolution of nanoscale roughness in Cu/SiO2 and Cu/Ta interfaces. Applied Physics Letters, 2012, 100, 024106.	1.5	7
493	Interplay between magnetism and chemical structure at spinel-spinel interfaces. Journal of Applied Physics, 2012, 111, 093903.	1.1	7
494	Controlling spin ordering in frustrated magnets via thin film heteroepitaxy. Physical Review B, 2012, 85, .	1.1	7
495	Compositional engineering of tin-lead halide perovskites for efficient and stable low band gap solar cells. , 2018, , .		7
496	Ptychography of Organic Thin Films at Soft X-ray Energies. Chemistry of Materials, 2019, 31, 4913-4918.	3.2	7
497	Kinetic origins of the metastable zone width in the manganese oxide Pourbaix diagram. Journal of Materials Chemistry A, 2021, 9, 7857-7867.	5.2	7
498	Stable Glasses of Organic Semiconductor Resist Crystallization. Journal of Physical Chemistry B, 2021, 125, 461-466.	1.2	7
499	Synchrotron xâ€ray diffraction studies of the lattice and magnetic structure of epitaxial Dy films in LaF3/Dy/LaF3sandwiches. Journal of Applied Physics, 1991, 70, 4465-4468.	1.1	6
500	<title>In-situ surface x-ray scattering of metal monolayers adsorbed at solid-liquid interfaces</title> . , 1991, 1550, 140.		6
501	Interfacial effects in thin films of polymeric semiconductors. Journal of Vacuum Science & Technology B, 2008, 26, 1454.	1.3	6
502	Surface structure of coherently strained ceria ultrathin films. Physical Review B, 2016, 94, .	1.1	6
503	Molecular engineering to improve carrier lifetimes for organic photovoltaic devices with thick active layers. Organic Electronics, 2017, 47, 57-65.	1.4	6
504	Crystal truncation rods from miscut surfaces. Physical Review B, 2017, 95, .	1.1	6

#	Article	IF	CITATIONS
505	Theoryâ€Guided Synthesis of a Metastable Leadâ€Free Piezoelectric Polymorph. Advanced Materials, 2018, 30, 1800559.	11.1	6
506	Synthesis and Crystallization of Atomic Layer Deposition β-Eucryptite LiAlSiO <sub>4</sub> Thin-Film Solid Electrolytes. ACS Applied Materials & Interfaces, 2020, 12, 56935-56942.	4.0	6
507	Twisted Aâ€Dâ€A Type Acceptors with Thermallyâ€Activated Delayed Crystallization Behavior for Efficient Nonfullerene Organic Solar Cells. Advanced Energy Materials, 0, , 2103957.	10.2	6
508	Why it is important to determine and report the impact of probe radiation. Joule, 2022, 6, 723-725.	11.7	6
509	Reaction-Mediated Transformation of Working Catalysts. ACS Catalysis, 2022, 12, 8007-8018.	5.5	6
510	Magnetization profile in antiferromagnetically coupled recording media. Applied Physics Letters, 2005, 86, 162506.	1.5	5
511	In situevolution of stress gradients in Cu films induced by capping layers. Applied Physics Letters, 2010, 96, 261903.	1.5	5
512	Self-assembly of cholesterol tethered within hydrogel networks. Polymer, 2016, 84, 371-382.	1.8	5
513	Advanced X-ray Scattering and Spectroscopy Characterization of an Antisoiling Coating for Solar Module Glass. ACS Applied Energy Materials, 2019, 2, 7870-7878.	2.5	5
514	High Power Energy Storage via Electrochemically Expanded and Hydrated Manganese-Rich Oxides. Frontiers in Chemistry, 2020, 8, 715.	1.8	5
515	Thickness Dependent Perpendicular Magnetic Domain Patterns in Sputtered Epitaxial FePt (001) L1 <sub>0</sub> Films. Materials Research Society Symposia Proceedings, 1998, 517, 319.	0.1	4
516	Mitigating residual stress in Cu metallization. Applied Physics Letters, 2012, 101, 231906.	1.5	4
517	Effect of Extensional Flow on the Evaporative Assembly of a Donor–Acceptor Semiconducting Polymer. ACS Applied Electronic Materials, 2019, 1, 2445-2454.	2.0	4
518	Morphology of Organic Semiconductors Electrically Doped from Solution Using Phosphomolybdic Acid. Chemistry of Materials, 2019, 31, 6677-6683.	3.2	4
519	Chemical Evolution of CoCrMo Wear Particles: An in Situ Characterization Study. Journal of Physical Chemistry C, 2019, 123, 9894-9901.	1.5	4
520	Organic thin-film microstructure characterization. , 2019, , 489-528.		4
521	Covalently Linked, Two-Dimensional Quantum Dot Assemblies. Langmuir, 2020, 36, 9944-9951.	1.6	4
522	Hybrid Nanostructured Ni(OH)2/NiO for High-Capacity Lithium-Ion Battery Anodes. Journal of Electrochemical Energy Conversion and Storage, 2020, 17, .	1.1	4

#	Article	IF	CITATIONS
523	Applications of synchrotron X-rays in microelectronics industry research. Nuclear Instruments & Methods in Physics Research B, 2005, 241, 247-252.	0.6	3
524	Effect of sintering conditions on mixed ionic-electronic conducting properties of silver sulfide nanoparticles. Journal of Applied Physics, 2012, 111, 053530.	1.1	3
525	Understanding stress gradients in microelectronic metallization. Powder Diffraction, 2012, 27, 92-98.	0.4	3
526	Multifunctional Optical Coatings and Light Management for Photovoltaics. , 2019, , 153-173.		3
527	Polyimideâ€PEG Segmented Block Copolymer Membranes with High Proton Conductivity by Improving Bicontinuous Nanostructure of Ionic Liquidâ€Doped Films. Macromolecular Chemistry and Physics, 2019, 220, 1900006.	1.1	3
528	Understanding Cu incorporation in the <mml:math xmlns:mml="http://www.w3.org/1998/Math/MathML"&gt;<mml:mrow><mml:msub><mml:mi>Cu</mml:mi><mml:r structure using resonant x-ray diffraction. Physical Review Materials, 2021, 5, .</mml:r </mml:msub></mml:mrow></mml:math 	ח <b>ר‱</b> < mi	ml <b>:ø</b> nn>2
529	Use of a Multiple Hydride Donor To Achieve an n-Doped Polymer with High Solvent Resistance. ACS Applied Materials & Interfaces, 2022, 14, 33598-33605.	4.0	3
530	Summary Abstract: Lowâ€energy electron diffraction study of the phases and phase transitions of oxygen physisorbed on graphite. Journal of Vacuum Science and Technology A: Vacuum, Surfaces and Films, 1984, 2, 898-898.	0.9	2
531	In Situ X-Ray Scattering of Monolayers Adsorbed at Electrochemical Interfaces Materials Research Society Symposia Proceedings, 1988, 143, 37.	0.1	2
532	Near-surface structure of aromatic polyimides: the effect of precursor isomers. Faraday Discussions, 1994, 98, 319.	1.6	2
533	Enrichment of Deuterium Oxide at Hydrophilic Interfaces in Aqueous Solutions. Langmuir, 2007, 23, 11943-11946.	1.6	2
534	Preparation of crystalline dielectric modification silane layer by spin-coating and its improvements on organic transistor performance. Proceedings of SPIE, 2009, , .	0.8	2
535	Operando Transmission X-ray Microscopy Studies on Li-Ion Batteries. Microscopy and Microanalysis, 2014, 20, 1526-1527.	0.2	2
536	Tunable mesoscale-structured self-assembled hydrogels synthesized by organocatalytic ring-opening polymerization. Polymer, 2015, 65, 93-104.	1.8	2
537	Understanding Chemomechanical Li-ion Cathode Degradation through Multi-Scale, Multi-Modal X-ray Spectromicroscopy. Microscopy and Microanalysis, 2018, 24, 426-427.	0.2	2
538	Thermodynamic guiding principles of high-capacity phase transformation materials for splitting H <sub>2</sub> O and CO <sub>2</sub> by thermochemical looping. Journal of Materials Chemistry A, 2022, 10, 3552-3561.	5.2	2
539	Light-induced halide segregation in perovskites with wrinkled morphology. Journal of Energy Chemistry, 2022, 71, 83-88.	7.1	2
540	X-ray scattering studies of the passive oxide film formed on iron. Synchrotron Radiation News, 1998, 11, 5-11.	0.2	1

#	Article	IF	CITATIONS
541	Ion Beam Stabilization of FePt Nanoparticle Arrays for Magnetic Storage Media. Materials Research Society Symposia Proceedings, 2003, 777, 651.	0.1	1
542	High-resolution x-ray analysis of graphene grown on 4H–SiC (000) at low pressures. Journal of Materials Research, 2014, 29, 439-446.	1.2	1
543	Development of a soft x-ray ptychography beamline at SSRL and its application in the study of energy storage materials. , 2015, , .		1
544	Simulation and characterization of cation disorder in \$\$hbox {ZnGeP}_{2}\$\$. Journal of Materials Research, 2022, 37, 1986-1996.	1.2	1
545	MBE Growth of Artificially-Layered Magnetic Metal Structures. , 1995, , 623-668.		0
546	Optoelectronic Devices: Ultrahigh Mobility in an Organic Semiconductor by Vertical Chain Alignment (Adv. Mater. 12/2016). Advanced Materials, 2016, 28, 2463-2463.	11.1	0
547	Operando X-Ray Diffraction for Characterization of Photovoltaic Materials. , 2017, , .		0
548	Using X-ray Spectromicroscopy for Operando Characterization of Li-S Batteries. Microscopy and Microanalysis, 2018, 24, 440-441.	0.2	0
549	Al tool makes phase identification crystal clear. Nature Computational Science, 2021, 1, 311-312.	3.8	0
550	X-Ray Studies of Energy Materials. , 2019, , 1-22.		0
551	X-Ray Studies of Energy Materials. , 2020, , 1803-1824.		0
552	Manipulation and statistical analysis of the fluid flow of polymer semiconductor solutions during meniscus-guided coating. MRS Bulletin, 0, , 1-14.	1.7	0
553	Cubic on the Streets, Tetragonal in the Sheets: The Two-Dimensional Nature of Dynamic Disorder in Hybrid Metal Halide Perovskite Semiconductors. , 0, , .		0
554	Increased crystallite size in thin films of C <sub>60</sub> and <i>p</i> -terphenyls <i>via</i> PDMS-assisted crystallization. Journal of Materials Chemistry C, 2022, 10, 5657-5665.	2.7	0
555	Phonons in Metal Halide Perovskites. , 2022, , 1-35.		0